Available online at www.sciencedirect.com

SCIENCE DIRECT®

Developmental Biology 286 (2005) 114 – 135

DEVELOPMENTAL BIOLOGY

www.elsevier.com/locate/ydbio

Formation of the digestive system in zebrafish: III. Intestinal epithelium morphogenesis

Annie N.Y. Ng[a,1], Tanya A. de Jong-Curtain[a,1], David J. Mawdsley[b,1], Sara J. White[a], Jimann Shin[b], Bruce Appel[b], P. Duc Si Dong[c], Didier Y.R. Stainier[c], Joan K. Heath[a,*]

[a]*Colon Molecular and Cell Biology Laboratory, Ludwig Institute for Cancer Research, Post Office Box 2008, Royal Melbourne Hospital, Parkville, Victoria 3050, Australia*

[b]*Department of Biological Sciences, Vanderbilt University, Nashville, TN 37235, USA*

[c]*Department of Biochemistry and Biophysics, University of California, San Francisco, CA 94143, USA*

Received for publication 11 September 2004, revised 30 June 2005, accepted 18 July 2005
Available online 24 August 2005

Abstract

Recent analysis of a novel strain of transgenic zebrafish (gutGFP) has provided a detailed description of the early morphological events that occur during the development of the liver and pancreas. In this paper, we aim to complement these studies by providing an analysis of the morphological events that shape the zebrafish intestinal epithelium. One of our goals is to provide a framework for the future characterization of zebrafish mutant phenotypes in which intestinal epithelial morphogenesis has been disrupted. Our analysis encompasses the period between 26 and 126 h post-fertilization (hpf) and follows the growth, lumen formation and differentiation of a continuous layer of endoderm into a functional intestinal epithelium with three morphologically distinct segments: the intestinal bulb, mid-intestine and posterior intestine. Between 26 hpf and 76 hpf, the entire intestinal endoderm is a highly proliferative organ. To make a lumen, the zebrafish endoderm cells undergo apical membrane biogenesis, adopt a bilayer configuration and form small cavities that coalesce without cell death. Thereafter, the endoderm cells polarize and differentiate into distinct cell lineages. Enteroendocrine cells are distinguished first at 52 hpf in the caudal region of the intestine in a new stable transgenic line, *Tg[nkx2.2a:mEGFP]*. The differentiation of mucin-containing goblet cells is first evident at 100 hpf and is tightly restricted to a middle segment of the intestine, designated the mid-intestine, that is also demarcated by the presence of enterocytes with large supranuclear vacuoles. Meanwhile, striking expansion of the lumen in the rostral intestine forms the intestinal bulb. Here the epithelium elaborates folds and proliferating cells become progressively restricted to a basal compartment analogous to the crypts of Lieberkühn in mammals. At 126 hpf, the posterior intestine remains an unfolded monolayer of simple columnar epithelium.
© 2005 Elsevier Inc. All rights reserved.

Keywords: Zebrafish; Endoderm; Intestine; Epithelium; Digestive system; Organogenesis; Enteroendocrine cell; Goblet cell; Enterocyte; GFP; *nkx2.2*

Introduction

The highly elaborate epithelial lining of the vertebrate alimentary canal develops from a thin ribbon of definitive endoderm that also gives rise to major cell types in other organs of the digestive system, including the pancreas, liver and gall bladder. In its mature form, the intestinal epithelium is a dynamic and self-renewing tissue system that encompasses most aspects of cell behavior. It comprises both rapidly proliferating, undifferentiated cells and differentiated cells of multiple lineages that are specialized to perform digestive, absorptive, protective and endocrine functions over a vast surface area. In the mammalian small intestine, epithelial homeostasis is maintained by balancing the self-renewal of stem cells, progenitor cell proliferation, cell fate-specific differentiation, cell migration and cell death in spatially distinct compartments that are aligned along a directional axis that originates at the base of pocket-like

* Corresponding author. Fax: +613 9341 3104.
E-mail address: joan.heath@ludwig.edu.au (J.K. Heath).
[1] These authors contributed equally to the paper.

0012-1606/$ - see front matter © 2005 Elsevier Inc. All rights reserved.
doi:10.1016/j.ydbio.2005.07.013

invaginations, called the crypts of Lieberkühn, and terminates at the tips of finger-like projections known as villi (Gordon and Hermiston, 1994; Sancho et al., 2003). In the mammalian small intestine, four cell lineages are derived from the descendants of a common multipotential stem cell. These progenitor cells undergo a series of binary cell fate decisions to give rise to the enterocytes, goblet, enteroendocrine and Paneth cells (Yang et al., 2001; Sancho et al., 2003; Schonhoff et al., 2004a,b). To a large extent, the genetic mechanisms involved in establishing and maintaining this constantly remodeling tissue system remain a mystery. However, our understanding of the underlying molecular mechanisms is likely to advance rapidly as increasing numbers of genetically modified mice and strains of mutant zebrafish with abnormal intestinal phenotypes become available for analysis.

Due to its many favorable characteristics, including prolific reproduction, external development and optical transparency of embryos, the zebrafish has become a well-established model for the genetic analysis of vertebrate organogenesis (Chen et al., 1996; Pack et al., 1996; Stainier et al., 1996; Drummond et al., 1998). Nevertheless, the deep internal position of the developing digestive system has made morphological analysis of this organ relatively difficult, particularly at early stages of development. The recent development of transgenic strains of zebrafish exhibiting tissue-specific patterns of green fluorescent protein (GFP) expression has transformed this situation. Of particular note is the gutGFP strain described by Field et al. (2003a,b), in which GFP expression is essentially restricted to endoderm and endoderm-derived organs from 22 h post-fertilization (hpf) through to adulthood. Studies conducted in this transgenic line have already provided novel insights into the morphogenesis of the liver and pancreas (Field et al., 2003a,b). Several transgenic lines have also been generated using the *intestinal fatty acid binding protein* (*ifabp*) promoter to drive GFP expression in the developing intestine, albeit not until 72 hpf (Her et al., 2004). In this paper, we introduce a new transgenic line, *Tg[nkx2.2a:mEGFP]*, which appears to be useful for studies of intestinal enteroendocrine cell development. In this line, the regulatory elements of the *nkx2.2a* gene drive strong EGFP expression in the brain, ventral neural tube and developing pancreas, as expected from previous studies (Qi et al., 2001; Sussel et al., 1998). In addition, EGFP expression is also present in a subset of cells scattered throughout the intestinal epithelium. These cells, which are *nkx2.2a* mRNA positive, exhibit the typical morphology of enteroendocrine cells and occur with the expected frequency and distribution of this hitherto difficult to visualize cell population in the intestinal epithelium. We show that a subset of these cells express both glucagon and somatostatin, confirming their identity as enteroendocrine cells.

In the developing zebrafish embryo, endoderm progenitor cells first become molecularly distinct at the late blastula stage (5 hpf) when dorsal and lateral cells at the blastoderm margin start to express *sox17* in response to the combined action of *casanova* (*cas*) (Kikuchi et al., 2001; Dickmeis et al., 2001; Warga and Stainier, 2002) and *spiel-ohne-grenzen* (*spg*)/*Pou2/Oct4* (Reim et al., 2004; Lunde et al., 2004). Nodal, a member of the TGFβ superfamily, provides an indispensable signal for this process in zebrafish and in all other vertebrates (Alexander and Stainier, 1999; Aoki et al., 2002; Schier, 2003; Stainier, 2002). Endoderm progenitor cells involute into the hypoblast, adopt a flattened morphology and express *foxA3/fkd2*, a definitive marker of endoderm (Warga and Kimmel, 1990; Warga and Nusslein-Volhard, 1999). The disorganized endoderm precursor cells extend filopodial processes to form a flattened and discontinuous layer of cells overlying the yolk. By 26 hpf, the cells have consolidated into a ribbon of tissue at the midline and subsequently adopt a bilayer configuration (Field et al., 2003a; Wallace and Pack, 2003) without first undergoing a transient stratified arrangement as occurs in mammals (Mathan et al., 1976). A few hours later, the cells establish apicobasal polarity in response to cell polarity and extracellular matrix signals (Horne-Badovinac et al., 2001; Wallace and Pack, 2003) and the intestinal lumen starts to form.

To complement previous studies of early gut development in zebrafish (Horne-Badovinac et al., 2001; Field et al., 2003a,b; Wallace and Pack, 2003), we now provide a detailed account of the morphogenetic events that take place during the formation of the intestinal epithelium. Our analysis focuses particularly on the period from around 26 hpf, when the endoderm precursor cells have converged to form the primitive gut, until 126 hpf when the intestine is functional and exotrophic nutrition begins. Our aim is to offer a framework for the future characterization of mutant phenotypes in which intestinal epithelial morphogenesis has been impaired. Such mutants are likely to provide insights into the regulation of processes such as intestinal epithelial cell proliferation, differentiation, migration and apoptosis. Interest in this area has intensified with the recognition that in humans the derailing of these basic developmental processes underlies a large variety of cancers, including colorectal cancer (Amatruda et al., 2002; Barolo and Posakony, 2002; Oving and Clevers, 2002).

Materials and methods

Generation of transgenic lines of zebrafish with specific patterns of GFP expression

The *Tg(gut GFP)s854* transgenic line (gutGFP) was generated by random integration into the host genome of a linearized construct (pESG) that encodes soluble (cytosolic) GFP downstream of the *Xenopus* elongation factor (EF)-1α promoter (Field et al., 2003a). To produce *Tg[nkx2.2a:mEGFP]* fish, a bacterial artificial chromosome (BAC) clone carrying the *nkx2.2a* locus was modified by *Esche-*

richia coli-based homologous recombination (Lee et al., 2001) and injected into embryos essentially as described previously (Shin et al., 2003). The transgene expresses a membrane-targeted form of EGFP (mEGFP), which was provided as a gift from David Turner and produced by fusing the Ras membrane localization (CAAX) sequence to the carboxyl terminus of EGFP. Full details of the transgene will be published elsewhere.

Embryo collection and live imaging

Zebrafish embryos were obtained from natural spawning in breeding colonies of either wild-type, *flotte lotte* (kind gift of the Max-Planck-Institute of Developmental Biology, Tübingen, Germany), gutGFP or *Tg[nkx2.2a:mEGFP]* fish kept on a 14-h light/10-h dark cycle according to standard procedures. Collected embryos were maintained in embryo medium (15 mM NaCl, 0.5 mM KCl, 1 mM $CaCl_2$, 1 mM $MgSO_4$, 0.15 mM KH_2PO_4, 0.05 mM NH_2PO_4, 0.7 mM $NaHCO_3$) at 28.5°C containing 0.003% 1-phenyl-2-thiourea (PTU, Sigma-Aldrich, St. Louis, MO) to inhibit melanin pigment formation and staged by morphological criteria (Kimmel et al., 1995). Embryos were dechorionated with watchmaker forceps or in bulk with 10 μg/ml pronase (Sigma-Aldrich).

Imaging of live gutGFP and *Tg[nkx2.2a:mEGFP]* transgenic embryos was carried out after anaesthetizing embryos with either 200 mg/l benzocaine (ethyl *p*-aminobenzoate; Sigma-Aldrich) solution or 150 mg/l tricaine (aminobenzoic acid ethyl ester; Sigma-Aldrich) solution in embryo medium. The fluorescent images of gutGFP embryos were obtained with an MRC-1024 confocal microscope (Bio-Rad Microscience Ltd. Hemel Hempstead, UK). Low magnification images of the trunk and intestinal tract of *Tg[nkx2.2a:mEGFP]* transgenic embryos were obtained with a Hamamatsu Orca cooled CCD digital camera (Hamamatsu City, Japan) mounted on a compound microscope with an FITC filter set. High magnification images of the intestinal tract were obtained by projecting optical section z-stacks collected with a Zeiss LSM510 Meta laser scanning confocal microscope (Gottingen, Germany) or a Nikon D-Eclipse C1 laser scanning confocal unit attached to a Nikon Eclipse TE2000-E inverted fluorescence microscope (Tokyo, Japan). Embryos for sectioning were embedded in 1.5% agar/5% sucrose and frozen in 2 methyl-butane chilled by immersion in liquid nitrogen. Sections (10 μm) were obtained using a cryostat microtome, mounted in 75% glycerol and imaged with a Zeiss LSM510 Meta laser scanning confocal microscope. All images were imported into CorelDRAW8. Image manipulation was limited to levels, hue and saturation adjustments.

Histology, immunohistochemistry and in situ hybridization

For histology, embryos were fixed in Bouin's solution overnight at 4°C and mounted in SeaPlaque 1% low-melting point agarose (FMC BioProducts, Rockland, ME). The blocks of embryos were dehydrated through a standard ethanol series to 100%, embedded in paraffin and sectioned at 5-μm intervals for staining with hematoxylin and eosin.

For immunohistochemistry of paraffin sections, antigen retrieval was performed before treating sections with 6% hydrogen peroxide in methanol and peroxidase blocking buffer (Zymed Laboratories, Inc., San Francisco, CA). Primary antibodies were mouse anti-BrdU (1:100 dilution; BD Biosciences, San Diego, CA), rabbit anti-human/mouse caspase 3 active (1:400 dilution; R&D Systems, Inc., Minneapolis, MN), mouse anti-cytokeratin (Pan) (1:200 dilution; Zymed Laboratories, Inc.) and mouse anti-E-cadherin (1:300 dilution; BD Biosciences). Secondary antibodies were ZyMax HRP-conjugated goat anti-mouse/anti-rabbit IgG (1:200 dilution; Zymed Laboratories, Inc.) or HRP-labeled polymer from the EnVision immunohistochemical kit (DAKO Corporation, Carpinteria, CA). The antibodies were visualized with 3,3′-diaminobenzidine tetrahydrochloride (DAB) substrate-chromagen (DAKO Corporation). Positive reactivity was revealed by the formation of a brown-colored precipitate at the site of the target antigen. Sections were counterstained lightly with hematoxylin. Negative controls were obtained by omitting primary antibodies. Sections were imaged on a Nikon Microphot FX upright microscope equipped with a SPOT cooled CCD camera (Diagnostics Instruments Inc., Sterling Heights, MI).

Frozen sections of *Tg[nkx2.2a:mEGFP]* transgenic embryos were prepared as described above and blocked in PBS containing 2% sheep serum and 2 mg/ml bovine serum albumen prior to being incubated with mouse anti-glucagon antibody (1:1000, Sigma-Aldrich) overnight at 4°C. Sections were washed in PBS and incubated overnight at 4°C with AlexaFluor 568 goat anti-mouse conjugate (1:500; Molecular Probes Inc., Eugene, OR) for fluorescent detection of antibody labeling. Slides were mounted in Vectashield mounting medium (Vector Laboratories, Inc., Burlingame, CA) and imaged using a Zeiss LSM510 Meta laser scanning confocal microscope.

For whole-mount immunohistochemistry, *Tg[nkx2.2a:mEGFP]* embryos were fixed in 2% formaldehyde in 0.1 M pipes, 1.0 mM MgSO4, 2 mM EGTA overnight at 4°C. The yolks were removed with watchmaker forceps and the embryos immersed in blocking buffer (4% BSA, 0.3% Triton X-100 PBS) for 1 h at 4°C. Primary antibodies were mouse anti-glucagon (1:1000 dilution) and rabbit anti-human somatostatin (1:1000 dilution; MP Biomedicals, Irvine, CA) diluted in blocking buffer and incubated overnight. The embryos were washed with 0.3% Triton X-100 PBS and incubated overnight at 4°C with fluorescent secondary antibodies (1:200 dilution, Alexa Fluor 568 goat anti-mouse and Alexa Fluor 647 goat anti-rabbit, Molecular Probes). Samples were mounted in Vectashield and imaged on a Zeiss LSM5 Pascal confocal microscope.

For whole-mount in situ hybridization, embryos were incubated in embryo medium with 0.003% phenylthiourea (PTU, Sigma-Aldrich) to prevent melanization, anaesthetized at 76 hpf and fixed in 4% paraformaldehyde/PBS at 4°C overnight. They were then dehydrated through a methanol/PBS series to 100% methanol and stored at −20°C. The embryos were rehydrated in PBS with 0.1% Tween 20 (PBST) and incubated with proteinase K (20 μg/ml; Roche Diagnostics, Mannheim, Germany) at RT for 60 min to allow penetration of the riboprobe. The embryos were then refixed in 4% paraformaldehyde/PBS at RT for 30 min and washed in PBST. Digoxygenin (DIG)-labeled riboprobe synthesis and in situ hybridization on rehydrated embryos were conducted as previously described (Hauptmann and Gerster, 2000). Sense and antisense riboprobes were synthesized by in vitro transcription using T3 and T7 polymerases and DIG-labeled UTP according to the manufacturer's instructions (Roche). The *nkx2.2a* sense and antisense riboprobes encompass the ORF of the *nkx2.2a* mRNA (Barth and Wilson, 1995). Hybridized riboprobes were detected using an anti-DIG antibody conjugated to alkaline phosphatase according to the manufacturer's instructions (Roche). No staining was observed when using the sense riboprobes. Removal of the yolk sac and yolk extension was performed manually with watchmaker forceps. Embryos were mounted in 70% glycerol/PBS and imaged using a QImaging Retiga Exi color CCD camera mounted on a compound microscope.

Detection of proliferating cells

To assess cell proliferation, live embryos were immersed in undiluted Cell Proliferation Labeling Reagent containing 5-bromo-2′-deoxyuridine (BrdU)/5-fluoro-2′-deoxyuridine (FdU) (Amersham Biosciences, Piscataway, NJ) for 30 min at 28.5°C. After several washes with prewarmed embryo medium, the embryos were left for a further 1 h at 28.5°C in fresh embryo medium before they were euthanized using 1000 mg/l benzocaine and fixed in Bouin's solution overnight at 4°C for embedding and sectioning. Detection of BrdU was carried out by immunostaining with a mouse anti-BrdU antibody (see above). All animal experiments were reviewed and approved by the Ludwig Institute/Department of Surgery-Royal Melbourne Hospital Animal Ethics Committee.

Detection of mucins using Alcian blue-periodic acid Schiff (AB–PAS) histochemical staining

Mucins and other carbohydrates secreted by intestinal goblet cells were demonstrated by sequentially placing deparaffinized and rehydrated sections in 1% Alcian blue pH 2.5 (Sigma-Aldrich) for 5 min, 1% aqueous periodic acid (Sigma-Aldrich) for 20 min and undiluted Schiff's reagent (Sigma-Aldrich) for 5 min. After washing in water, the sections were counterstained lightly with hematoxylin, dehydrated and mounted. Using this method, acidic mucins stain blue, neutral mucins and other carbohydrates red and acidic and neutral mucins together stain purple.

Mapping of the integration site of the GFP construct in gutGFP fish

Genomic sequences flanking the GFP-containing construct (pESG) that was used to generate the gutGFP founder fish were obtained using the Advantage Genomic PCR Kit (Clontech Laboratories, Inc., Palo Alto, CA) according to the manufacturer's instructions. Three adaptor-ligated genomic libraries were constructed using 1 μg of digested (*Pvu*II, *Dra*I or *Hind*III) genomic DNA extracted from adult gutGFP zebrafish tissues. The first round of PCR amplification was carried out using the supplied anchor oligonucleotide, AP1 and an oligonucleotide specific to the GFP sequence (either the GFP forward primer F1: 5′-CATGGCCAACACTTGTCACT-3′ or the GFP reverse primer R1: 5′-AAAGGGCAGATTGTGTGGAC-3′). This was followed by a nested PCR using the supplied nested oligonucleotide, AP2 and a nested oligonucleotide specific to the GFP sequence (GFP forward nested primer F2: 5′-AAGCCAACTTCAAGACCCGCCACAA-3′ or GFP reverse nested primer R3: 5′-AGATGGTCCTCTCCTGCACGTATCCCTC-3′). Specific products were subjected to nucleotide sequencing. Based on the sequence obtained, additional oligonucleotide primers were designed so that outlying flanking sequences could be amplified. This process was repeated until endogenous genomic DNA flanking the construct was obtained. A PCR product encompassing 185 bp of host genomic sequence downstream of the GFP cDNA was amplified using the following primers: forward primer RH1: 5′-GCGAATGGGGACTGAAAGAGTG-3′ and reverse primer RH2: 5′-ACCACATGCAGAGGTTGCAAAA-3′ and subjected to radiation hybrid analysis using the T51 GoodFellow Panel to map its position in the zebrafish genome. Results from the radiation hybrid mapping were submitted to http://zfrhmaps.tch.harvard.edu/ZonRHmapper for assignment of linkage group.

Results

In gutGFP transgenic embryos, the pattern of GFP fluorescence provided an overall picture of the morphogenesis of the zebrafish alimentary canal from 26 hpf onwards. To reveal cellular detail along the entire length of the digestive tract from mouth to anus, sagittal histological sections were employed. Transverse sections were used to highlight the position of the intestine in the dorsal–ventral axis, especially in relation to its neighboring tissues including the yolk, liver, swim bladder, pancreas and pronephric ducts.

Formation of the primitive gut

At 26–30 hpf, the cells that will give rise to the primitive gut comprise a continuous thin layer of endoderm just above the dorsal surface of the yolk at the midline of the embryo (Fig. 1A, white arrows; Fig 1B, yellow dashed lines; Fig. 1D, black arrows). The endoderm tissue extends from a site close to where the mouth will form (Fig. 1B, left white arrow; Fig 1D, white arrowhead) to the position of the future anus (Fig. 1A, right white arrow; Fig. 1D, black arrowhead). GFP expression, which is otherwise restricted to the endoderm by 22 hpf, is also present in the hatching gland (Fig. 1A, yellow arrow) and notochord (Fig. 1B, n) at 26 hpf. Endoderm ventral to the first two somites and adjacent to the developing pectoral fin buds (Fig. 1D middle black arrow, Fig. 1F, dotted white lines) comprises a solid mass of cells from which the developing liver (Fig. 1B, black arrowhead), pancreas (Fig. 1B, white arrowhead) and swim bladder will develop. Transverse sections through a rostral region of the endoderm, ventral to the hindbrain, reveal a broad, elliptical expanse of cells extending laterally across the embryo (Fig. 1E, dotted lines), which we will hereafter refer to as the "pharyngesophageal" endoderm, that will eventually give rise to the mouth, pharynx and esophagus. In a caudal region near the end of the yolk extension, a much smaller mass of endoderm is seen, flanked by a pair of

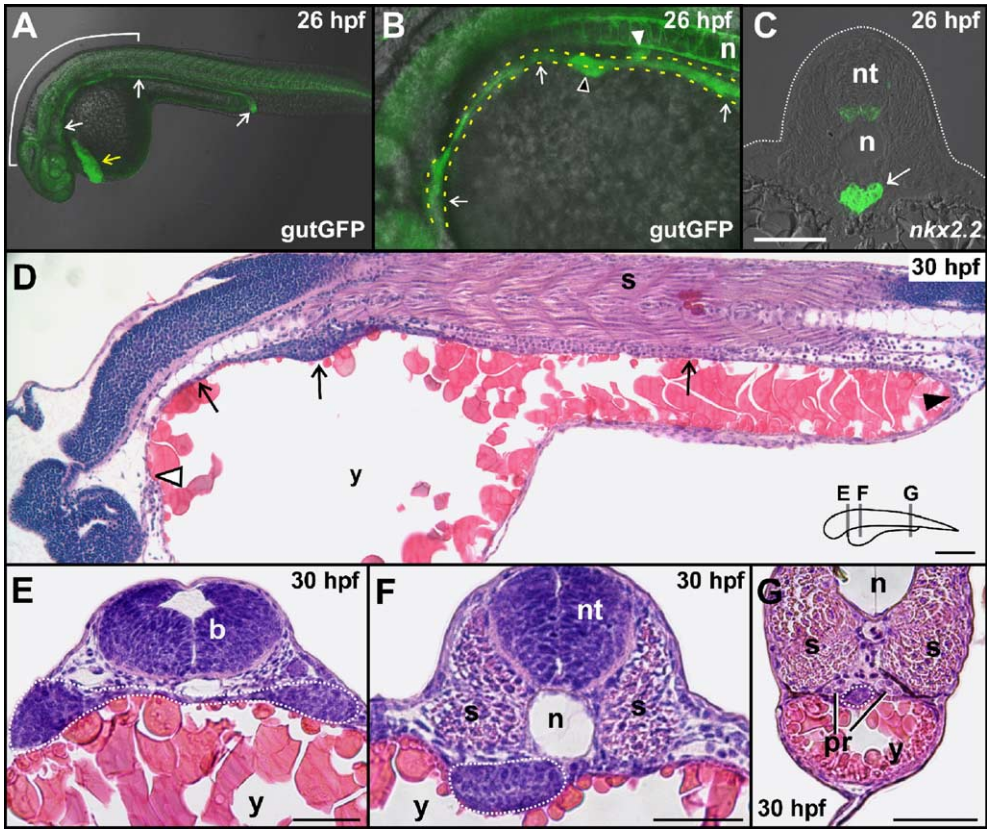

Fig. 1. Formation of the primitive gut at 26–30 hpf. The digestive system in zebrafish is derived from a thin, continuous layer of endoderm (A, B). Expression of GFP in gutGFP transgenic embryos was visualized at 26 hpf using confocal microscopy. Except where stated otherwise, dorsal is to the top, rostral is to the left. Panels A and B are brightfield and fluorescence composites of lateral views. Panel A is a thick optical section and panel B is a two-dimensional projection of a confocal stack of the bracketed region shown in panel A. (A) The previously ubiquitous GFP expression pattern in gutGFP embryos is largely restricted to the primitive gut (white arrows) and hatching gland (yellow arrow). (B) The yellow dotted lines follow the path of a thin layer of endoderm lying at the midline of the embryo extending from a site close to where the mouth will form (left white arrow) to the position of the future anus (A, right white arrow). Two small aggregates of cells corresponding to the nascent liver (B, black arrowhead) and the caudal bud of the pancreas (B, white arrowhead) are visible. The notochord (n) is also positive. (C) Transverse section of a *Tg[nkx2.2a:mEGFP]* embryo at 26 hpf. The first detectable EGFP fluorescence in endodermal tissue is in the developing pancreas at 26 hpf (arrow). Fluorescence is also seen in the ventral neural tube (nt). (D) Histological analysis of sagittal sections of 30 hpf zebrafish larvae reiterates the picture seen in (A, B). A thin ribbon of endoderm residing on the dorsal surface of the yolk at the midline of the embryo (black arrows) extends from a site close to where the mouth will form (white arrowhead) to the position of the future anus (black arrowhead). A bulge in the endoderm adjacent to the first few somites (middle black arrow) corresponds to the region where the liver, pancreas and swim bladder anlagen will form. (E–G) Transverse sections through the endoderm at three different regions (see schematic drawing in panel D) reveal disorganized masses of cells only a few cells thick (outlined with dotted lines) with no lumen. (E) Transverse section through the pharyngesophageal endoderm reveals a broad elliptical mass of cells that spans the entire width of the embryo. The lateral bulges of endoderm will give rise to the future pharyngeal arches. (F) Endoderm ventral to the first few somites and adjacent to the developing pectoral fin buds comprises a solid mass of cells from which the developing intestine, liver, pancreas and swim bladder will emerge. (G) A thin rod of endoderm cells in the region of the embryo near the end of the yolk extension is flanked by a pair of developing pronephric ducts (pr), both containing a small lumen. b, brain; n, notochord; nt, neural tube; s, somite; y, yolk. Scale bars, 50 μm (C–F).

developing pronephric ducts (Fig. 1G). In contrast to the pronephric ducts, in which a lumen is already formed, no lumen is present yet in the primitive gut endoderm and the cells do not display any apparent signs of radial arrangement. Analysis of EGFP expression in transverse sections of *Tg[nkx2.2a:mEGFP]* transgenic embryos at 26 hpf revealed restricted EGFP fluorescence in the pancreatic primordium (Fig. 1C, white arrow) and the ventral neural tube (Fig. 1C, nt). EGFP expression was absent in other parts of the embryo.

Stage I: Lumen formation

The period from 26 hpf to 52 hpf is a phase of rapid intestinal morphogenesis. By 52 hpf, several cell masses associated with the developing gut are clearly seen (Fig. 2A, bracketed region). These correspond to the developing pharyngeal arches (left white arrow), liver, pancreas and swim bladder. This region is expanded in the projection shown in Fig. 2B. Here, the developing liver (black arrowhead) and swim bladder (white arrowhead) are particularly prominent while the pancreas, positioned on the right side of the embryo, is largely obscured. The developing intestinal tube (yellow dashed lines) and pharyngeal arches (left white arrow) are continuous with each other. Histological analysis of the endoderm at 52 hpf also reveals a continuous ribbon of tissue extending from the position of the future mouth (Fig. 2C, white arrowhead) to the position of the future anus at the end of the yolk extension (Fig. 2C, black arrowhead). The liver and swim bladder anlagen are conspicuous structures, situated at the level of the first few somites (Fig. 2C). While the endoderm in the pharyngesophageal region still appears as a broad expanse of cells extending laterally across the embryo (Fig. 2D, dotted lines), the cells in the rostral region of the primitive intestine have consolidated into a structure with a lumen on the left side of the embryo (Fig. 2E, dotted lines). In the same section, the developing pancreas is seen on the right, ventral and adjacent to the swim bladder, which occupies a more dorsal position at the midline of the embryo and also contains a lumen. In a more caudal region of the intestinal tract the thinner rod of endoderm has undergone radial arrangement and a small lumen is seen (Fig. 2F). Examination of sagittal sections of the endodermal layer in the pharyngesophageal and intestinal regions at high magnification (Fig. 2G, dotted lines) and serial transverse sections at the junction of the two regions (data not shown) confirmed that these tissues are continuous with each other. The location of the connection of the liver to the intestinal tube (hepatic duct) provides a useful topographical landmark to grossly divide the endodermal layer into two main regions (Field et al., 2003a). Endoderm rostral to the hepatic duct corresponds to the pharyngesophageal region. Within this region, the swim bladder is connected to the dorsal endoderm via the pneumatic duct (Fig. 2B, yellow arrowhead) and provides a marker for the future esophagus (Fig. 2H). Meanwhile, endoderm adjacent to and caudal to the hepatic duct gives rise to the primitive intestine. As noted previously by others (Pack et al., 1996), the esophagus is connected directly to the intestine in the stomachless zebrafish. This organization is different from the majority of vertebrates, including mammals, chicks, frogs and the adult forms of most teleost fish. However, the larval forms of most teleost fish also do not possess a stomach. Only in fish of the family Cyprinidae, of which the zebrafish is a member, is the stomach absent at all stages (Noaillac-Depeyre and Gas, 1976; Rombout et al., 1985). Instead of a stomach, cyprinids develop an expanded structure in the rostral segment of the intestine, known as the intestinal bulb, which acts as the major site of lipid and protein digestion (Rombout et al., 1985). The cecum, a conspicuous structure at the junction between the small and large intestines in mammals and chicks, is also missing in zebrafish.

Lumen formation is initiated in the region of the future esophagus and the rostral end of the intestinal tract (intestinal bulb primordium) and thereafter advances caudally through the intestine (Figs. 2I–K). The cuboidal endoderm cells first adopt a bilayer configuration. Initially, several small cavities are formed (Fig. 2J), eventually coalescing to create a more extensive lumen, as seen in the intestinal bulb primordium (Fig. 2I). In contrast to the process in higher vertebrates, the intestinal endoderm of zebrafish does not adopt a transient stratified epithelial organization. As the lumen is formed, the lining endoderm cells are immediately arranged into a monolayer configuration. Lumen formation in the pharyngeal endoderm is also initiated in the rostral region (position of the future mouth) and advances towards the esophagus. During the third day of development, the lumen in the pharyngesophageal region becomes continuous with the lumen in the intestinal tract.

To determine whether lumen formation involved the elimination of cells by apoptosis, the expression of the active, cleaved form of caspase 3, an effector caspase active during the advanced stages of apoptosis (for a review, see Chang and Yang, 2000), was investigated at 52 hpf using immunohistochemistry. No apoptotic cells or cell debris were detected in the developing lumen of either the pharyngesophageal region (Fig. 3A) or the intestinal tract (Figs. 3B and C) and there was no anti-active caspase 3 activity in the endoderm/epithelial cells throughout this region. These observations suggest that tubular morphogenesis in the zebrafish pharynx, esophagus and intestinal tract is independent of programmed cell death. Indeed, in contrast to mammals, where concerted patterns of apoptosis are required for the formation of a monolayer of intestinal epithelium (Abud et al., 2005), the use of active caspase 3 immunohistochemistry revealed that cell death is a rare event during the first 2 weeks of normal zebrafish intestinal development. However, this was not the case in a small number of zebrafish intestinal mutants we examined, including *flotte lotte* (*flo*; Chen et al., 1996), where caspase

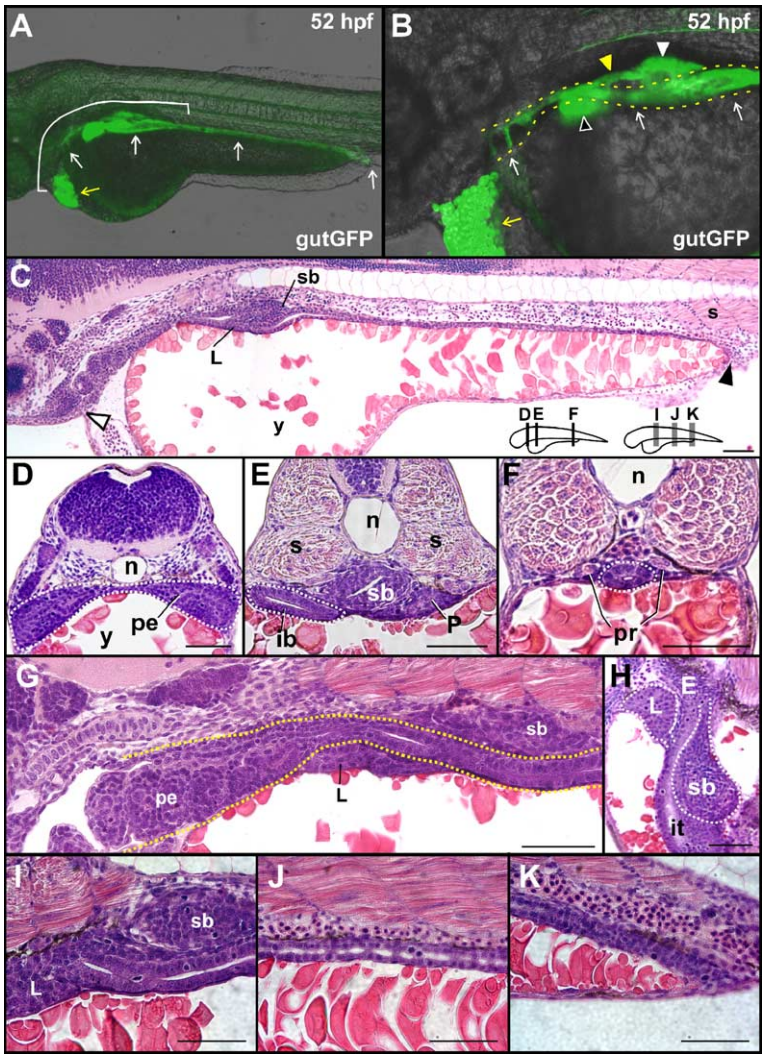

Fig. 2. Digestive organ morphogenesis and formation of the intestinal lumen at 54 hpf. (A–B) Expression of GFP in gutGFP transgenic embryos was visualized at 52 hpf. Images are brightfield and fluorescence composites viewed in the confocal microscope. Panel A is a thick optical section and panel B is a two-dimensional projection of a confocal stack of the bracketed region shown in panel A. (A) The GFP expression pattern is restricted to the primitive gut (white arrows) and hatching gland (yellow arrow). (B) The yellow dotted lines outline the layer of endoderm and demonstrate that the pharyngesophageal and intestinal regions are clearly continuous. Morphogenesis has resulted in a number of conspicuous structures. The developing pharyngeal arches (left white arrow), nascent liver (black arrowhead) and the dorsally positioned swim bladder (white arrowhead) are clearly visible and their connections to the primitive intestinal tract are evident. The developing pancreas lying on the right side of the embryo is largely obscured in this view. (C–K) Histological analysis of gut development at 54 hpf. (C) The gut endoderm extends from the position of the future mouth (white arrowhead) to the future anus (black arrowhead). (D–F) Transverse sections as shown in the schematic in panel C highlight differences in the gross morphology of the endoderm. (D) The pharyngesophageal endoderm (pe) is spread across the width of the embryo (outlined with dotted lines). (E) The endoderm adjacent to the pectoral fin bud has undergone morphogenesis to form the intestinal tract (it; dotted lines), swim bladder (sb) and pancreas (P). (F) The caudal endoderm (dotted lines) is radially arranged and contains a small lumen. (G) Sagittal section at the junction between the pharyngesophageal and intestinal endoderm shows that these two regions are continuous with each other (dotted yellow lines). (H) Coronal section showing the liver and intestinal tract (it) on the left side of the embryo. The developing swim bladder occupies a dorsal position at the midline. At this stage, the connection of the liver to the endoderm (hepatic duct) roughly divides the digestive tract into two regions. Endoderm rostral to the hepatic duct corresponds to the pharyngesophageal region that will eventually give rise to the mouth, pharynx and esophagus. Within the pharyngesophageal region, the swim bladder is connected to the dorsal endoderm via the pneumatic duct and provides a marker for the esophagus (E). Meanwhile, endoderm adjacent to and caudal to the hepatic duct will give rise to the intestine. (I–K) Sagittal sections as shown in the schematic in panel C. Endodermal cells adopt a bilayer configuration and separate to form a central lumen. Lumen formation progresses from the intestinal bulb primordium (I) to the middle segment (J) and then the caudal segment (K) of the intestinal tract. Initially several small cavities are formed as shown in panel J; these coalesce to create a more extensive lumen as seen in panel I. n, notochord; pr, pronephric ducts; s, somite; y, yolk. Scale bars, 50 μm (C–K).

3-positive apoptotic cells were readily detected in the intestinal lumen from 96 hpf (Fig. 9H).

To test whether apical surface biogenesis is involved or coincident with lumen formation, we performed immunohistochemistry with pan-cytokeratin antibodies at 52 hpf. Expression of cytokeratin was detected at the apical surface of cuboidal endodermal cells at the onset of lumen formation, both in the pharyngesophageal region (Figs. 3D

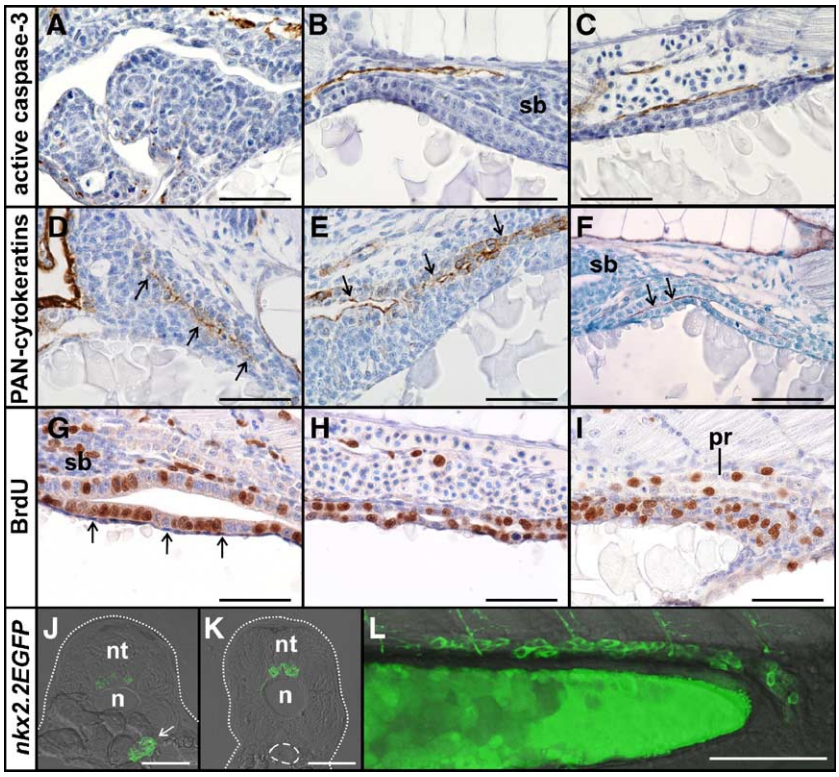

Fig. 3. Cell death, cell proliferation and apical membrane morphogenesis during intestinal lumen formation. All embryos were 52 hpf except panel D, which was 36 hpf. All panels are sagittal sections. (A–C) Immunostaining with antibodies to the active, cleaved form of caspase 3 reveals no apoptotic cells in the pharyngesophageal region (A), intestinal bulb primordium (B) and a middle segment of the intestine (C) during lumen formation. Meanwhile, the liver, pronephric ducts and specific regions of the brain were positive for caspase 3 immunostaining (data not shown). (D–F) Immunostaining with pan-cytokeratin antibodies reveals cytokeratin expression at the apical surface of endodermal cells in the pharyngesophageal region (D, E) and intestinal bulb primordium (F). Within the pharyngesophageal region, expression of cytokeratins appears to be coincident with onset of lumen formation, overlapping precisely with cell positions in which the future lumen will form (arrows in panel D). (G–I) BrdU incorporation assays indicate that the intestinal tract is an actively proliferating organ at this stage of development, with cells within S-phase of the cell cycle densely scattered throughout the intestinal bulb primordium (G), a rostral segment (H) and caudal segment (I) of the intestinal tract. (J–L) Appearance of EGFP-positive cells in the intestinal tract of *Tg[nkx2.2a:mEGFP]* zebrafish embryos at 52 hpf. (J, K) Transverse sections of *Tg[nkx2.2a:mEGFP]* embryos, (L) lateral image of live *Tg[nkx2.2a:mEGFP]* embryo. (J) EGFP expression in the developing pancreas, now on the right of the embryo, remains strong at 52 hpf (arrow). At 52 hpf, a further population of EGFP-positive cells emerges in the caudal intestinal epithelium (L). These EGFP-positive cells are not present in a region of more rostral intestinal epithelium (K, outlined by dashed line). Axons extending down from the neural tube are also evident (L). n, notochord; nt, neural tube; pr, pronephric ducts; sb, swim bladder. Scale bars, 50 μm (A–K) and 100 μm (L).

and E, arrows) and in the primitive intestinal tract (Fig. 3F, arrows) and was coincident with the onset of lumen formation, overlapping precisely with cell positions in which the future lumen will form.

To assess the proliferation of intestinal endodermal/epithelial cells at 52 hpf, we performed bromodeoxyuridine (BrdU) incorporation analysis to mark cells progressing through the S-phase of the cell cycle. Our results demonstrate that at this stage of development the intestinal tract is a highly proliferative organ, with cycling cells densely scattered throughout the entire intestinal tract (Figs. 3G–I). The cells of the pronephric ducts were also proliferating (Fig. 3I). At this stage, cells from the lateral plate mesoderm have started to encircle the primitive intestine (Fig. 3G, arrows). These cells will proliferate and differentiate into connective tissue that will give rise to the muscle layers. While this process is hard to discern by histology at this stage of intestinal development, gene expression studies have revealed that it is already populated with enteric neuron progenitors and smooth muscle progenitor cells at 48 hpf (Shepherd et al., 2004; Wallace et al., 2005a,b).

Analysis of EGFP fluorescence in transverse sections of *Tg[nkx2.2a:mEGFP]* transgenic fish at 52 hpf is clearly evident in the pancreatic primordium, now positioned on the right side of the embryo (Fig. 3J), and the ventral neural tube (Figs. 3J and K). EGFP expression was absent in most regions of the developing intestinal tube (Fig. 3K, dashed line) but, somewhat unexpectedly, scattered oval-shaped EGFP-expressing cells were noticed at 52 hpf in the most caudal region of the developing intestine (Fig. 3L). Further analysis (see below) suggests that these cells correspond to enteroendocrine cells.

Stage II: Epithelial cell polarization

By 74–76 hpf, the entire digestive tract is a hollow tube (Fig. 4A). While at the rostral end, the mouth has opened and a single continuous lumen from mouth to anus is

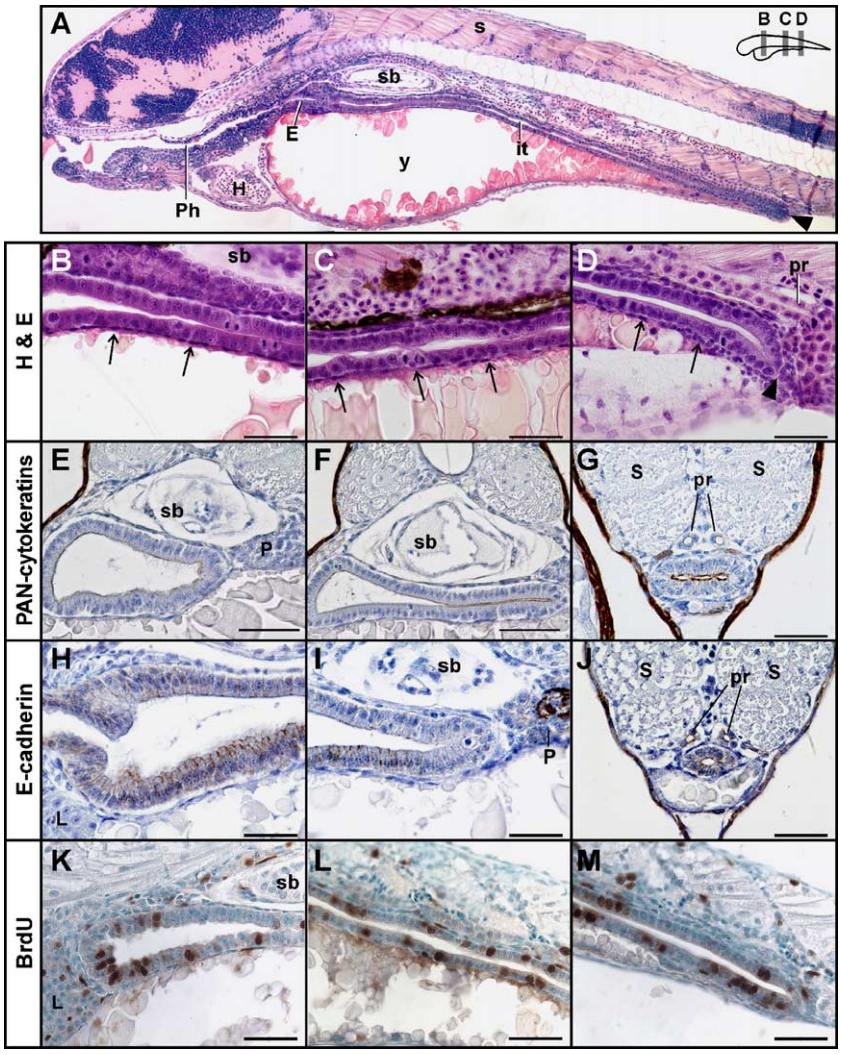

Fig. 4. Polarization of the intestinal epithelium at 74–76 hpf. (A) Lumen formation is complete and the intestinal tract is a hollow tube. At the rostral end, the mouth has opened but the anus will remain closed until a day later. (B–D) Sagittal sections at the regions shown in the schematic drawing in panel A, corresponding to the intestinal bulb primordium (B), a middle segment of the intestinal tract (C) and a caudal segment of the intestinal tract (D), demonstrate that the endodermal cells throughout the length of the intestinal tract are polarizing into columnar epithelium. (E–G) Transverse sections of the same three regions were immunostained with pan-cytokeratin antibodies. Prominent expression is observed at the apical surface of polarized epithelial cells throughout the length of the intestinal tract. Cells separating or cells that had just separated to form a lumen show more intense expression (F, G). (H–J) Immunostaining with E-cadherin antibodies demonstrates expression on the lateral membranes of the polarized epithelia in the intestinal bulb primordium (H, sagittal section; I, transverse section) and the caudal end of the intestine (J, transverse section). The highest level of E-cadherin expression was found in cells on the ventral side directly in contact with the yolk (H, I). Other cells that express E-cadherin include a central region in the pancreas (I) and the pronephric ducts (J). (K–M) BrdU incorporation into epithelial cells in the intestinal bulb primordium (K), a middle segment of the intestinal tract (L) and the caudal end of the intestine (M) demonstrated high proliferative activity throughout the intestinal tract. E, esophagus; H, heart; it, intestinal tract; P, pancreas; Ph, pharynx; pr, pronephric ducts; sb, swim bladder; s, somite; y, yolk. Scale bars, 50 μm (B–M).

Fig. 5. Remodeling of the intestinal epithelium and terminal differentiation of epithelial cells at 98–102 hpf. (A, B) Left and right lateral views of gutGFP larvae at 98 hpf. Images are brightfield and fluorescence composites viewed in the confocal microscope. The tissue-specific GFP expression pattern facilitates the visualization of the morphology of the digestive organs, the intestine (white arrows), liver (black arrowhead) and pancreas (white arrowhead) in live zebrafish embryos. (C) With the opening of the anus, the intestinal tract at 102 hpf is now a completely open-ended tube lined by a monolayer of polarized epithelial cells. The lumen in the most rostral region of the intestinal tract has expanded to form the intestinal bulb (ib). (D) Nascent folds (arrows) appear in the intestinal bulb. (E) Differentiation of goblet cells (arrowheads) in the middle segment of the intestinal tract demarcates the mid-intestine (see also K). In adjacent enterocytes, large supranuclear vesicles are visible. (F) Cells in the caudal segment, designated the posterior intestine, remain columnar and unfolded. (G–I) BrdU incorporation assays reveal that proliferative cells are now restricted to the base of the folds in the intestinal bulb (G, arrows), and there is a marked reduction in cell proliferation in the mid-intestine (H). Cells in the posterior intestine remain proliferative (I). (J–L) Histochemical staining with Alcian blue and periodic acid Schiff reagent (AB–PAS) reveals that goblet cells located in the rostral segment of the posterior intestine (K) synthesize only acidic mucins (turquoise staining). Meanwhile, the intestinal bulb (J) and the caudal segment of the posterior intestine (L) are devoid of goblet cells. (M–P) In *Tg[nkx2.2a:mEGFP]* embryos at 100 hpf, EGFP-positive cells are seen along the entire rostrocaudal length of the intestinal tract, from intestinal bulb to anus (M, arrows). The EGFP-positive cells in both the intestinal bulb (N) and the mid-intestine (O) extend a prominent process. (P) The body of an EGFP-positive cell is adjacent to the basement membrane (bm) and extends its process to the luminal surface. am, apical membrane; lu, lumen; a, anus; G, gill arches; L, liver; sb, swim bladder; s, somite;. y, yolk. Scale bars, 50 μm (C–L, O), 250 μm (M), 100 μm (N) and 25 μm (P).

formed, the anus remains closed (Figs. 4A and D). Coincident with the opening of the lumen, the second stage of intestinal morphogenesis, characterized by polarization of the cells of the intestinal epithelium, ensues (Figs. 4B–D). The epithelial cells adopt a columnar shape and the cell nuclei are situated towards the base of the cells. A thin layer of mesenchymal tissue is visible around the epithelium (Figs. 4B–D, arrows). Expression of cytokeratins at the apical membrane of the epithelial cells remains prominent (Fig. 4E), with expression appearing more intense in cells that are in the process of separating to form a lumen or have just separated (Figs. 4F and G). Polarization is also evident by the expression of the adherens junction protein, E-cadherin on the lateral membranes of the cells (Figs. 4H–J) with cells on the ventral side of the developing intestinal bulb staining more prominently for E-cadherin than on the dorsal side (Figs. 4H and I). A central region in the pancreas also stains positively for E-cadherin (Fig. 4I), corresponding to the membranes of clustered endocrine cells in the islet (Dahl et al., 1996). Weak expression of E-cadherin is also detected in cells at the most caudal end of the intestinal tract that are not yet fully polarized (Fig. 4J). Cells lining the

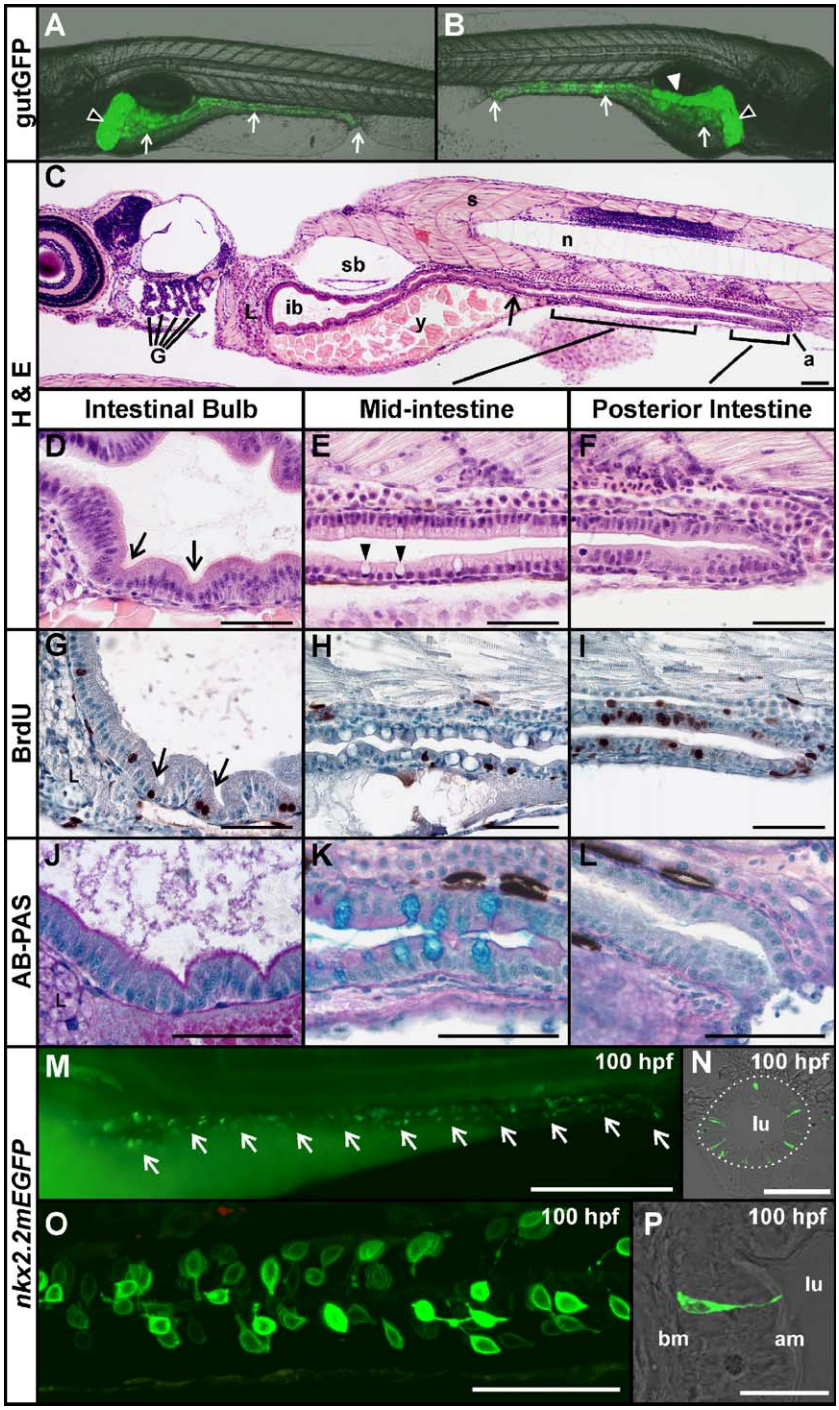

pronephric ducts also express E-cadherin. Meanwhile, the epithelial cells continue to proliferate throughout the rostrocaudal axis of the intestinal tract, as shown by the high frequency of cells that have incorporated BrdU (Figs. 4K–M).

Stage III: Remodeling and differentiation of the intestinal epithelium

By the end of the fourth day of development the intestinal tract has undergone extensive remodeling. At 98 hpf, GFP expression is entirely restricted to the digestive organs (Figs. 5A and B, white arrows) and the thin lining of the inflated swim bladder (barely discernible). Intense fluorescence is seen in the developing liver in left and right lateral views of the embryo (Figs. 5A and B, black arrowheads) and in the pancreas in right lateral views (Fig. 5B, white arrowhead). This tissue-specific GFP expression pattern is maintained throughout development and into adulthood. With the opening of the anus, the intestine becomes a completely open-ended tube lined by a monolayer of polarized epithelium (Fig. 5C). Stage III intestinal morphogenesis is associated with compartmentalization of the intestinal tract into three main segments: the intestinal bulb (Fig. 5D), mid-intestine (Fig. 5E) and posterior intestine (Fig. 5F). Within each segment, cells acquire characteristics that are likely to reflect their specialized functions.

Elaboration of folds in the intestinal bulb

By the end of the fourth day, the most rostral region of the intestinal tract has undergone a striking expansion in the diameter of the luminal space to adopt a rounded appearance and form the structure known as the intestinal bulb (Figs. 5C and D). The epithelial lining of the intestinal bulb starts to develop invaginations or folds (Fig. 5D, arrows). Epithelial folding extends caudally to the level where the intestinal tube realigns with the midline of the embryo (Fig. 5C, arrow).

Restricted proliferation and differentiation of goblet cells and enteroendocrine cells

In contrast to the random pattern of BrdU incorporation observed during the first 3 days of development, BrdU incorporation at 102 hpf is progressively restricted to the nuclei of cells positioned at the base of the nascent folds in the intestinal bulb (Fig. 5G, arrows). Interestingly, markedly reduced cell proliferation is detected in the middle segment of the intestinal tract (Fig. 5H), while the cells in the posterior intestine remain proliferative (Fig. 5I). In parallel with the reduced rate of cell proliferation, the middle segment of the intestinal tract becomes a region of extensive cell differentiation characterized by the appearance of cells with large goblet-shaped vacuoles (Figs. 5E and H). In order to determine whether these cells correspond to mucus-secreting goblet cells, tissue sections were stained histochemically with Alcian blue and periodic acid Schiff's reagent (AB–PAS). These two stains discriminate between acid (turquoise) and neutral (red) mucin subtypes, respectively. Cells containing large deposits of acidic mucins (Fig. 5K, turquoise staining) are conspicuous only in the middle segment of the intestine (Figs. 5J–L). We also noticed that the non-goblet cells in this region contain large vacuoles in the supranuclear cytoplasm (Fig. 5E) that are not seen in the enterocytes elsewhere. Thus, the mid-intestine is demarcated by the early development of goblet cells and enterocytes with large vacuoles in the supranuclear cytoplasm. Meanwhile the intestinal bulb (Fig. 5J) and the posterior intestine (Fig. 5L) are devoid of goblet cells.

At 74 hpf (data not shown), 100 hpf (Fig. 5M, arrows) and 125 hpf (Fig. 6A), EGFP-fluorescing cells in *Tg[nkx2.2a:mEGFP]* transgenic embryos are evident along the entire rostrocaudal length of the intestinal tract, from intestinal bulb to anus. Confocal analysis of transverse sections demonstrated that these cells are contained within the epithelial layer (Fig. 5N). The EGFP-positive cells display a distinctive morphology. While the main part of the cell body is adjacent to the basement membrane, the cells extend a prominent process to the luminal surface (Figs. 5O and P).

The occurrence of EGFP-fluorescing cells in the intestinal epithelium was unexpected. Previous studies of zebrafish *nkx2.2a* expression using in situ hybridization had focused on the brain and neural tube and the presence of *nkx2.2a*-positive cells in the intestinal epithelium was not reported (Barth and Wilson, 1995; Schäfer et al., 2005). To determine whether our observations of EGFP expression in the intestinal epithelium of *Tg[nkx2.2a:mEGFP]* embryos represented an authentic component of the *nkx2.2a* expression pattern, we conducted further in situ hybridization experiments on wild-type embryos at 74 hpf. Our experiments demonstrate unequivocally that cells expressing *nkx2.2a* mRNA are scattered throughout the zebrafish intestinal epithelium with the same frequency and distribution as the EGFP-fluorescing cells in the *Tg[nkx2.2a:mEGFP]* line (Figs. 6B–E). Expression of *nkx2.2* mRNA was also observed in the brain, ventral neural tube (Figs. 6B, D and E) and pancreas (Figs. 6B and C, white arrowheads), as expected.

The morphology of the *nkx2.2a/EGFP*-positive cells is typical of the open type of enteroendocrine cells that have been well characterized in higher vertebrates (for a review, see Montuenga et al., 2003), other stomachless teleost fish (Pan et al., 2000; Kamisaka et al., 2003) and invertebrates (Neves et al., 2003). This prompted us to investigate whether the *nkx2.2a/EGFP*-positive cells expressed any of the hormones that are typically produced by mammalian enteroendocrine cells. Using antibodies raised to mammalian intestinal hormones, we were able to detect glucagon (Figs. 6H and L) and somatostatin (Fig. 6K) in a small

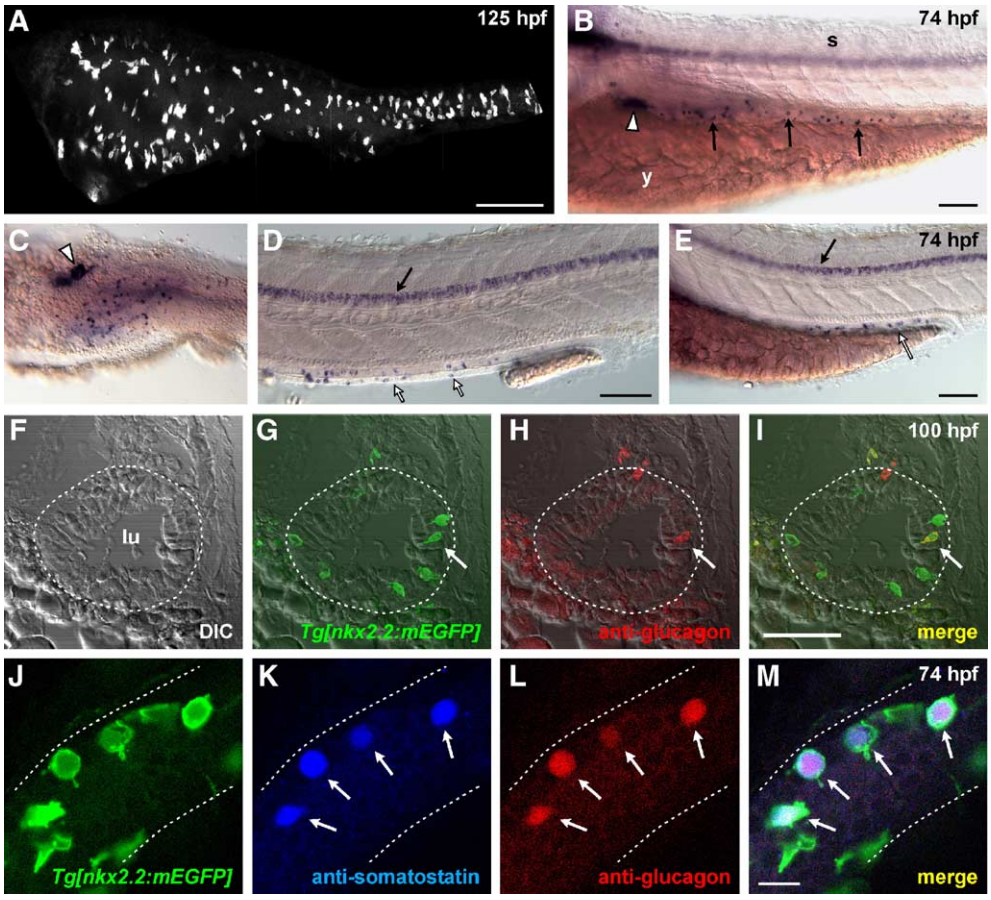

Fig. 6. The EGFP-positive cells in the intestinal epithelium of *Tg[nkx2.2a:mEGFP]* embryos express *nkx2.2a* mRNA and gut hormones. (A) Confocal projection showing EGFP-positive cells throughout the zebrafish intestine at 125 hpf. Rostral to the left. Scale bar, 200 μm. (B–E) A population of *nkx2.2a* mRNA-expressing cells, with the same density and distribution as the EGFP-positive cells, is scattered throughout the intestinal epithelium at 74 hpf. (B) Lateral view of the rostral region of the intestine (intestinal bulb primordium) showing *nkx2.2a* mRNA expression in the pancreatic anlage (white arrowhead) and in scattered intestinal epithelial cells (black arrows). (C) Ventral view of the intestinal bulb primordium with the yolk removed. *nkx2.2a* mRNA expression is present in scattered intestinal epithelial cells on the left of the midline and in the pancreatic anlage on the right (white arrowhead). (D, E) Lateral views of more caudal regions of the intestine with (D) and without (E) the yolk removed. The presence of *nkx2.2a* mRNA expression is clearly visible in cells spanning the monolayer of intestinal epithelium (white arrows). A stripe of cells in the ventral neural tube is also positive (black arrow). Scale bars, 100 μm. (F–M) A proportion of EGFP-positive cells in *Tg[nkx2.2a:mEGFP]* embryos at 74 hpf and 100 hpf express glucagon and somatostatin. (F–I) Transverse sections through the intestinal bulb region of *Tg[nkx2.2a:mEGFP]* embryos at 100 hpf stained for glucagon using immunohistochemistry. (F) DIC image, (G) composite image of DIC and EGFP fluorescence (green), (H) composite image of DIC and glucagon fluorescence (red), (I) Images shown in panels G and H merged. A single EGFP-positive cell (arrow) in this section synthesizes glucagon. Scale bar, 50 μm. lu, lumen: s, somite; y, yolk. (J–M) Lateral views of the intestinal bulb region of *Tg[nkx2.2a:mEGFP]* embryos at 74 hpf stained for glucagon and somatostatin using whole-mount immunohistochemistry. (J) EGFP fluorescence (green), (K) somatostatin fluorescence (blue), (L) glucagon fluorescence (red), (M) Images shown in panels J, K and L merged. Four of the EGFP-positive cells in this view synthesize both glucagon and somatostatin (arrows). Scale bar, 25 μm.

subset (5–7%) of *nkx2.2a/EGFP*-positive cells throughout the intestinal tract at both 74 hpf and 100 hpf. Interestingly, the same cells that express somatostatin also express glucagon (Figs. 6K–M), in contrast to what we found in the zebrafish pancreatic islet, where these two hormones are expressed by distinct populations of cells, as observed in mammals (data not shown). Thus, anti-glucagon antibodies specifically mark cells at the extreme periphery of the pancreatic islet, while anti-somatostatin and anti-insulin antibodies label two further populations of cells within the pancreatic islet (data not shown). At this stage, we do not know whether the co-localization of glucagon and somatostatin in a small fraction of zebrafish enteroendocrine cells at 74–100 hpf is a permanent characteristic of this subpopulation of cells or is a transient event during development. The fact that enteroendocrine cells first become visible in the posterior intestine before appearing in the intestinal bulb and mid-intestine is also interesting since it contrasts markedly with the general rostral-to-caudal wave of morphogenesis and differentiation that otherwise takes place in the developing zebrafish (and mammalian) intestine.

Formation of a functional gut

After 5 days of development, the alimentary canal comprises the mouth, pharynx, esophagus, intestinal bulb, posterior intestine and anal opening. The yolk is completely

resorbed (Fig. 7A). Within the intestinal bulb, the epithelial folding is more extensive (Fig. 7B) while the mid-intestine and posterior intestine remain unfolded (Figs. 7C and D). The patterns of proliferation in the intestinal epithelium resemble those observed 1 day earlier, with proliferation restricted to cells positioned at the base of the folds in the intestinal bulb (Fig. 7E, arrows) and little or no proliferation in the mid-intestine (Fig. 7F). At this stage, the posterior intestine also shows a low rate of proliferation (Fig. 7G). The presence of goblet cells remains restricted to the mid-intestine (Figs. 7C, arrows and I, turquoise staining) as do the enterocytes containing large vacuoles in the supra-nuclear cytoplasm (Figs. 7C and I, arrowheads). A layer of thickened mesenchymal tissue surrounding the intestinal epithelium is readily detected in most sections (for example, see Fig. 7I, arrows).

At 2 weeks, the intestine is still essentially a straight tube and folding of the intestinal epithelium has advanced throughout the intestinal tract (Fig. 8A). This process proceeds in a rostrocaudal direction as in mammals, with folds in the mid-intestine first appearing at around 8 dpf and in the posterior intestine at around 12 dpf (data not shown). The morphological characteristics of the intestinal epithelium consolidate into three distinct compartments. In the intestinal bulb, the tall folds (plicae) look villus-like in sagittal (Fig. 8B) and transverse (Fig. 8E) sections and the epithelial cells have a dense cytoplasm. Throughout the mid- and posterior intestine, the progressively shorter folds almost completely occlude the (narrower) lumen (Figs. 8C, D, F, G). BrdU incorporation analysis shows that only cells positioned at the base of the folds are proliferating in all regions of the intestine, including the intestinal bulb (Fig. 8H, arrows), the mid-intestine (Fig. 8I, arrows) and the posterior intestine (Fig. 8J). Thus, the proliferative compartments at the base of intestinal folds in zebrafish are highly analogous to the crypts of Lieberkühn in the mature mammalian intestine, as noted previously in other cyprinids, including grass carp (Stroband and Debets, 1978) and *Barbus conchonius* (Rombout et al., 1984). At 14 dpf, goblet cells are observed in all three regions of the

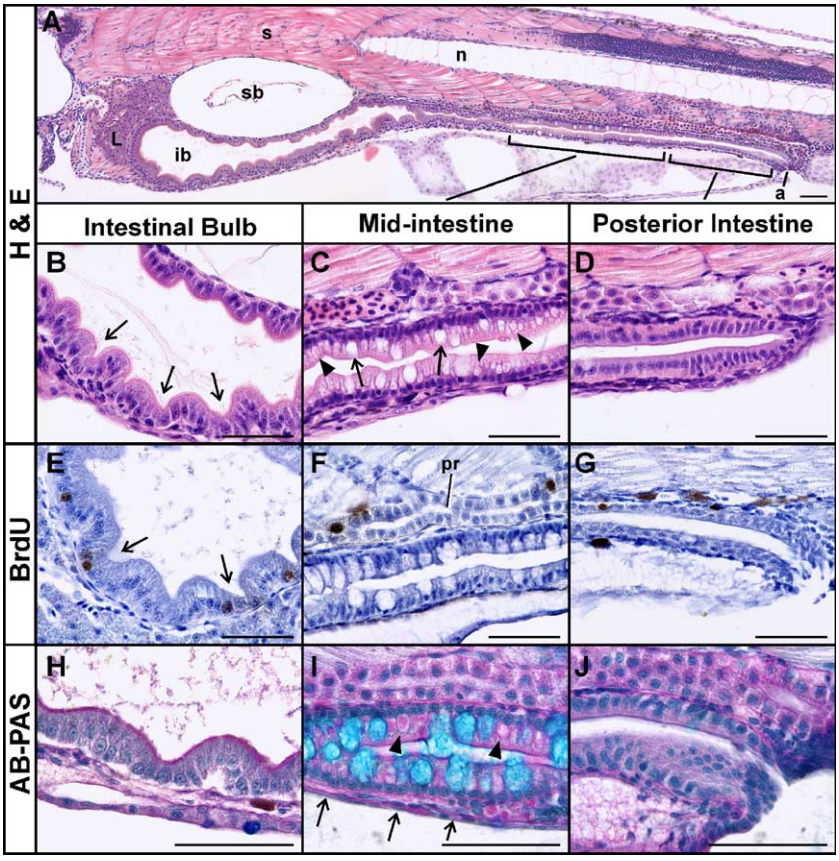

Fig. 7. The functional intestinal epithelium. (A) Sagittal section of the intestine at 126 hpf reveals three compartments. Resorption of the yolk is complete and the animal must now survive by exotrophic nutrition. (B–D) Folding of the epithelium is extensive in the intestinal bulb (B, arrows) while the epithelium in the mid-intestine and posterior intestine remains unfolded (C, D). The mid-intestine is demarcated by the presence of goblet cells (C, arrows) and enterocytes with large supranuclear vesicles (C and I, arrowheads). (E–G) Patterns of proliferation in the intestinal epithelium resemble those observed at 102 hpf, with proliferation restricted to cells positioned at the base of the folds in the intestinal bulb (E, arrows) and little or no proliferation in the mid-intestine (F). Cells in the posterior intestine also show reduced rates of proliferation (G). (H–J) Histochemical staining with Alcian blue and periodic acid Schiff's base reagent (AB–PAS) demonstrates that goblet cells continue to synthesize acidic mucins (I, turquoise staining). A layer of mesenchymal tissue surrounding the intestinal epithelium is evident in a number of sections (for example, panel I, arrows). a, anus; ib, intestinal bulb; L, liver; n, notochord; pr, pronephric ducts; s, somite; sb, swim bladder. Scale bars, 50 μm.

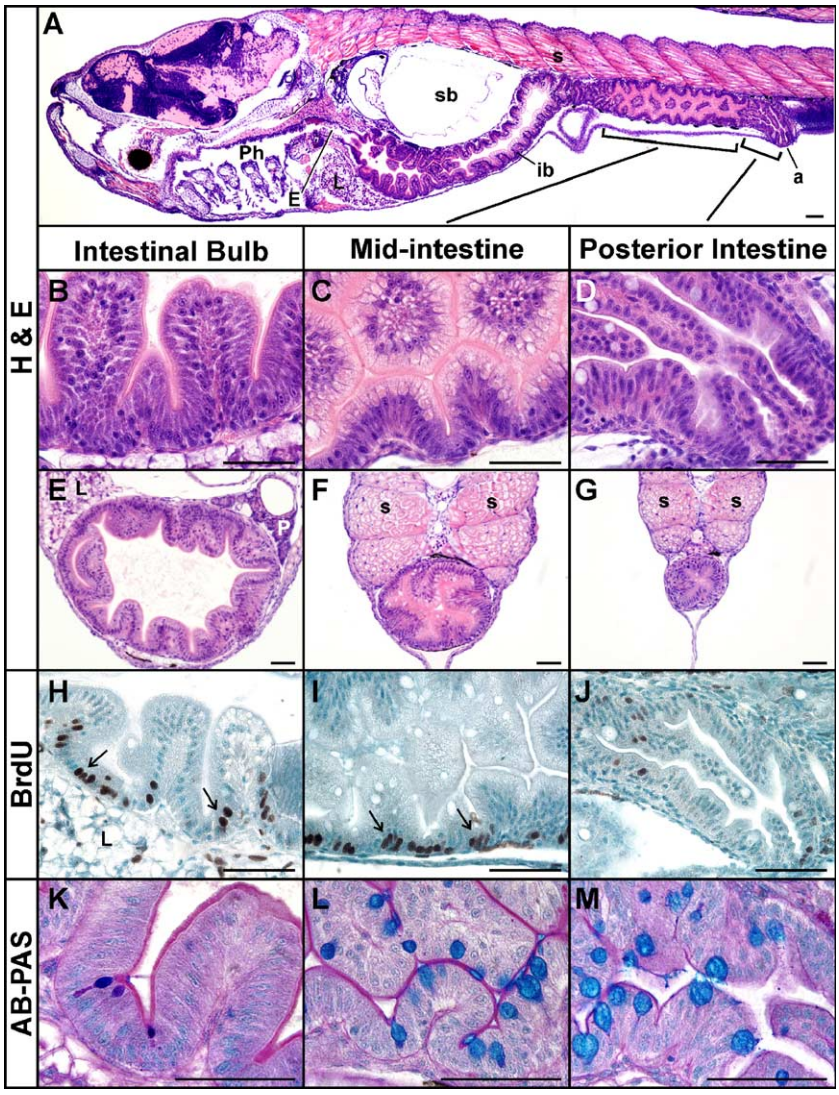

Fig. 8. The entire juvenile alimentary canal at 14 dpf. Panels A to J show sagittal (A–D, H–M) and transverse (E–G) sections taken at three different regions of the intestine. Panels B, E, H and K correspond to the intestinal bulb; panels C, F, I and L to the mid-intestine; and panels D, G, J and M to the posterior intestine. (A) Epithelial folding has advanced throughout the intestinal tract. (B–G) Three distinct regions are observed. In the intestinal bulb, the folds (plicae) are conspicuously tall and the epithelial cells have a dense cytoplasm (B, E). In the mid-intestine the folds are short and stumpy and almost completely occlude the lumen (C, F). There are large supranuclear vacuoles in the enterocytes. The folds in the posterior intestine (D, G) are shorter than those found in the intestinal bulb and mid-intestine. (H–J) BrdU incorporation demonstrates that only cells positioned at the base of the folds (arrows in H and I) are proliferating in all regions of the intestine. (K–M) Histochemical staining with Alcian blue and periodic acid Schiff's base reagent (AB–PAS) demonstrates that goblet cells within the intestinal bulb secrete both acidic and neutral mucins (K, purple staining). Goblet cells in the mid-intestine (L) and posterior intestine (M) secrete only acidic mucins (turquoise staining). a, anus; E, esophagus; L, liver; ib, intestinal bulb; P, pancreas; Ph, pharynx; s, somite; sb, swim bladder. Scale bars, 50 μm.

intestinal tract. In the intestinal bulb, only a few scattered goblet cells are present and these secrete both acidic and neutral mucins (Fig. 8K, purple staining). By now, both the mid-intestine and the posterior intestine contain abundant numbers of goblet cells, all producing acidic mucins (Figs. 8L and M, turquoise staining). However, enterocytes containing large supranuclear vacuoles remain restricted to the mid-intestine (Fig. 8C). We also looked for Paneth cells using phloxine–tartrazine staining. Paneth cells are a fourth enterocyte lineage found specifically at the base of crypts in the mammalian small intestine. They secrete anti-bacterial proteins such as lysozyme and defensins and are thought to play a role in protecting the stem cells that reside directly above them (for a review, see Ganz, 2003). Their secretory granules characteristically stain bright red with phloxine–tartrazine. We found no evidence for the existence of Paneth cells in the zebrafish intestinal epithelium either during development or in adulthood (data not shown) as noted by others (Pack et al., 1996). Paneth cells are also absent in frogs and, to our knowledge, have not been reported yet in chicks, which is perhaps surprising in view of the general similarity between the organization of the chick and mammalian small intestines.

One of the purposes of this study was to provide a morphological atlas of zebrafish intestinal epithelium development against which existing and future intestinal mutants could be compared. The *flotte lotte* (*flo*) mutant is one of a small number of intestinal development mutants that was identified on the basis of abnormal morphology during the first large-scale mutagenesis screen in Tübingen (Chen et al., 1996). As shown previously (Fig. 4), the intestinal epithelium in wild-type embryos at 76 hpf is a monolayer of polarized (columnar) cells (Fig. 9A). At the same stage, intestinal epithelial cells in *flo* embryos are largely cuboidal (Fig. 9B, black arrows) and a number of nuclei are found in positions away from the basement membrane (Fig. 9B, arrowheads). At 100 hpf, BrdU incorporation assays revealed markedly fewer proliferating cells in the intestinal bulb epithelium of *flo* embryos compared to wild-type siblings (Figs. 9C and D). We also noted at this stage that even after AB–PAS staining, goblet cells could not be discerned in the mid-intestinal epithelium of *flo* embryos (Figs. 9E and F). By 126 hpf, the intestinal epithelial cells in *flo* embryos remain unpolarized and a number of cells have rounded up, detached from the basement membrane and are present in the lumen (Fig. 9H, arrows). The detached rounded cells stain positively for active caspase 3 (Fig. 9J, arrows) confirming that these cells are undergoing apoptosis. This is in marked contrast to the frequency of cell death in the intestinal epithelium of wild-type zebrafish where apoptotic cells are rarely detected from 26 hpf to 14 dpf.

Mapping of the construct integration site in gutGFP transgenic fish

With the aim of delineating the mechanism underlying the tissue-specific GFP expression pattern in the gutGFP line, we mapped the site where the transgenic construct had integrated into the host genome. First, we used Southern analysis to establish that the expression construct had integrated into a single site in the genome of the founder fish (data not shown). We then used inverse PCR to isolate genomic DNA flanking the construct. Using the BLAST algorithm, a 185-bp genomic segment that shared no homology with sequences in the zebrafish genome database was selected for radiation hybrid mapping. The resulting data positioned the GFP integration site on linkage group 18 close to EST fa11c04 with a highly significant LOD score of 18.431, distance 3cR. This EST corresponds to a sequence in the 3′UTR of the *foxA3/fkd2* gene. We found that the *foxA3/fkd2* gene is located on zebrafish BAC clone, ZK223N17, 58 kb away from the construct integration site and oriented in the opposite direction.

Discussion

Our morphological analysis of intestinal formation in zebrafish revealed three main stages of development: Stage I: from hatching to the opening of the mouth, involved the conversion of a thin ribbon of endoderm into a tubular structure; Stage II: from opening of the mouth to the opening of the anus, marked the proliferation and polarization of the intestinal epithelium; Stage III: from the opening of the anus to the complete resorption of the yolk, involved remodeling, compartmentalization and differentiation of the intestinal epithelium. Salient features of these three stages are schematically represented in Fig. 10.

All the organs of the digestive tract, including the pharynx, esophagus, liver, pancreas and intestine, arise from a continuous layer of endoderm

The serendipitous GFP expression pattern in the gutGFP line greatly facilitates the visualization of the developing gut, liver and pancreas in early zebrafish embryos. At 26 hpf, we were able to discern a thin continuous ribbon of fluorescent endoderm all the way from the position of the future mouth to the future anus (Fig. 1A). We did not see any morphological evidence for different parts of the digestive tract developing independently from this cord of endoderm. However, different regions of this tissue already exhibit differential patterns of gene expression by this stage of development (Wallace and Pack, 2003). Also at this time, the endoderm cells caudal to the level of the first somite move towards the midline where they consolidate into a solid rod (Field et al., 2003a; Ober et al., 2003). This concerted cell movement contrasts with the behavior of cells within the endoderm layer rostral to the first somite, which instead remain spread across the width of the developing organism. Transverse sections through the primitive digestive system at 30 hpf reveal aggregates of disorganized endodermal cells that are individually morphologically indistinguishable from one another along its entire length (Figs. 1D–G; Horne-Badovinac et al., 2001; Wallace and Pack, 2003). Shortly thereafter, the layer of endoderm converts into a tubular structure.

Cavitation of the endoderm layer into a tubular gut without cell loss

The mechanism of lumen formation in the zebrafish intestine differs markedly from that described for higher vertebrates. In mouse and chick embryos, the folding of an initially flat layer of endoderm forms the intestinal lumen. The rostral and caudal extremes of the endoderm move ventrally and laterally towards each other until they fuse to form a blind-ended tube of stratified endoderm (reviewed by Wells and Melton, 1999; Grapin-Botton and Melton, 2000; Tam et al., 2003). In contrast, zebrafish lumen formation is achieved by a wave of cavitation that is initiated in the region of the future esophagus and intestinal bulb and advances into the posterior intestine (Horne-Badovinac et al., 2001; Wallace and Pack, 2003). In zebrafish, lumen

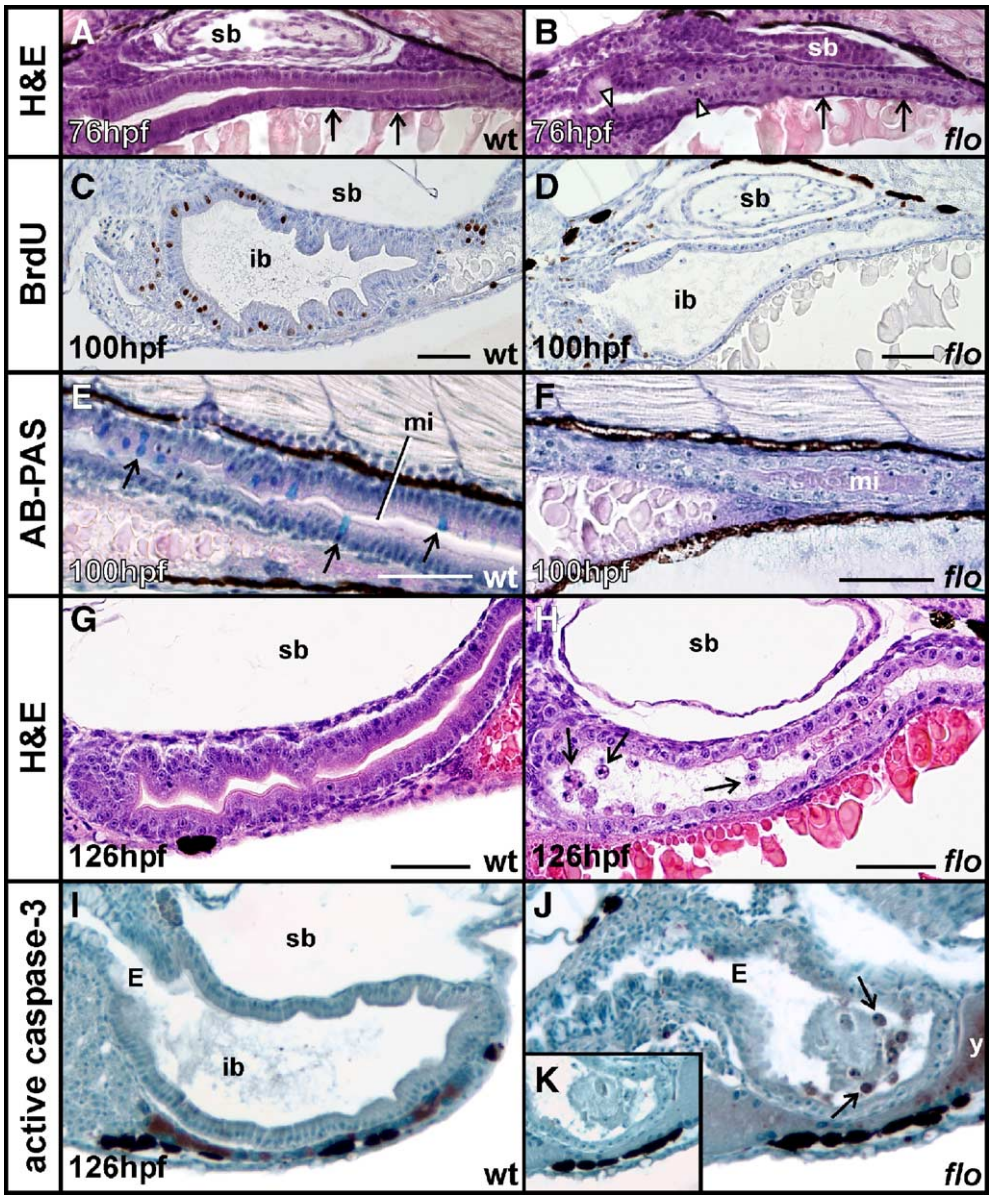

Fig. 9. Morphological abnormalities in the intestinal epithelium of *flotte lotte* (*flo*) embryos. (A, B) Transverse sections of the intestinal epithelium in wild-type (sibling) and *flo* embryos at 76 hpf. Whereas in wild-type embryos, the intestinal epithelial cells are polarized and cell nuclei are positioned adjacent to the basement membrane (A, arrows), intestinal epithelial cells in *flo* embryos are largely cuboidal (B, black arrows) and several cell nuclei are located in positions away from the basement membrane (B, arrowheads). (C) Epithelial cell proliferation in wild-type embryos at 100 hpf is becoming restricted to cells positioned at the base of folds in the intestinal bulb (brown nuclei); however, there is little or no proliferation in the same region of *flo* embryos (D). (E–F) Histochemical staining with Alcian blue and periodic acid Schiff's base reagent (AB–PAS) demonstrates the presence of goblet cells in the mid-intestine of wild-type embryos (E, arrows) but not in the mid-intestine of *flo* embryos (F). Sagittal sections of the intestinal epithelium in wild-type (G) and *flo* (H) embryos at 126 hpf stained with H&E. The intestinal epithelium in wild-type embryos is a monolayer of polarized cells that is elaborating folds (G) while the intestinal epithelium in *flo* embryos comprises an unfolded monolayer of cuboidal cells (H). A number of cells with condensed nuclei have rounded up and detached from the basement membrane (H, arrows). (I, J) Sagittal sections of the intestinal epithelium in wild-type (I) and *flo* (J) embryos at 126 hpf stained for active caspase 3 using immunohistochemistry. The detached rounded cells in the intestinal lumen of *flo* embryos show brown staining (J, arrows) confirming that these cells are undergoing apoptosis. No apoptotic cells are detected in the intestine of wt embryos (I). (K) Adjacent (control) section to panel J processed for active caspase 3 immunohistochemistry omitting the primary antibody contains no brown staining. E, esophagus; ib, intestinal bulb; L, liver; mi, mid-intestine; sb, swim bladder; wt, wild-type; y, yolk. Scale bars, 50 μm.

formation by cavitation has also been implicated in the morphogenesis of the inner ear (Haddon and Lewis, 1996; Whitfield et al., 2002) and neural tube (Strahle and Blader, 1994). However, unlike these other organ systems in which surplus cells in the center of the cellular mass are eliminated by apoptosis, our analysis revealed that creation of the luminal space in the intestinal tract occurred without programmed cell death. Lumen formation without cell loss, or "cord hollowing" (Lubarsky and Krasnow, 2003), also takes place in the formation of the *Caenorhabditis elegans*

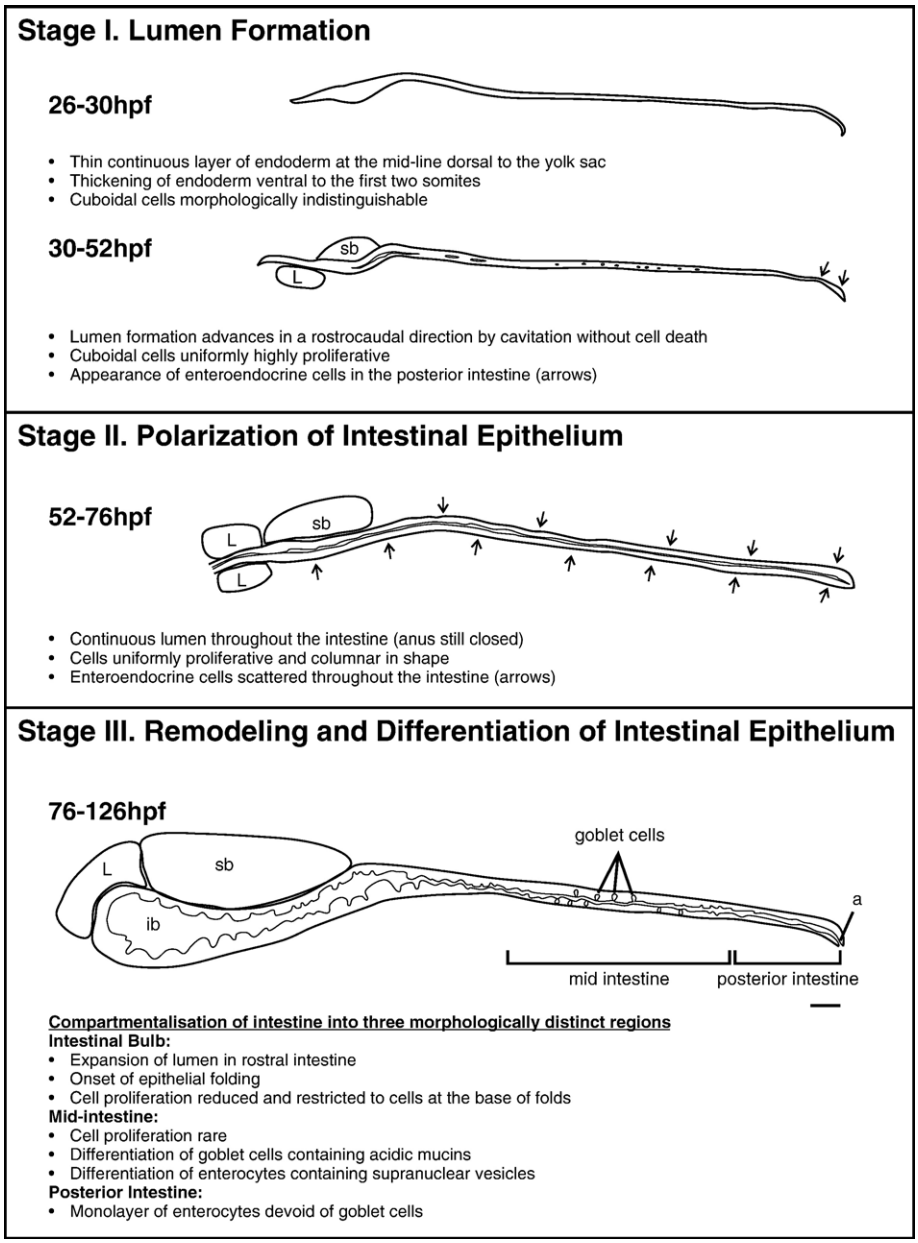

Fig. 10. Schematic drawings depicting the salient features of zebrafish intestinal formation over the first 5 days of development. ib, intestinal bulb; L, liver; sb, swim bladder. Scale bar, 50 μm.

intestine (Leung et al., 1999) and the chambers of the *Drosophila* heart (Rugendorff et al., 1994). It has been proposed that one mechanism through which a lumen may be formed without cell loss is apical membrane biogenesis (Lubarsky and Krasnow, 2003). Evidence that this process is important in the tubulogenesis of the zebrafish intestine was provided by analysis of the *heart and soul* (*has*) mutant (Stainier et al., 1996). The *has* embryos have defects in intestinal lumen formation and contain a null mutation in the gene encoding a cell polarity signaling molecule, atypical protein kinase Cλ (Horne-Badovinac et al., 2001). Our demonstration that the onset of apical cytokeratin expression overlapped precisely with the position of the future lumen is also consistent with the notion that apical membrane biogenesis plays a key role in the cavitation process. Other molecules in addition to cytokeratins may also be involved in establishing cell polarity; for instance, Type I laminin and β-actin form a basal ring around the endodermal cells at this stage of gut development (Wallace and Pack, 2003).

Formation of a monolayer of intestinal epithelium

In mammals, the conversion of a rapidly proliferating stratified layer of endoderm into a monolayer of polarized epithelial cells involves the selective apoptosis of superficial cells lining the lumen and the progressive restriction of cell proliferation to cells adjacent to the basement membrane (Mathan et al., 1976; Abud et al., 2005). This occurs as a

rostral-to-caudal wave of morphogenesis and results in the formation of profuse invaginations in the epithelial surface into which proliferating cells progressively become restricted and is concomitant with the development of finger-like projections, the nascent villi. By 126 hpf, the appearance of the zebrafish intestinal epithelium in the intestinal bulb region is highly reminiscent of that seen in embryonic mammals. However, in contrast to mammals, we saw no evidence that cell death was involved in shaping the zebrafish intestinal epithelium during this time. Further remodeling of the mammalian intestinal epithelium after birth results in the formation of the crypts of Lieberkühn, deep pocket-like invaginations in the epithelial surface into which proliferative cells become further restricted. In zebrafish, there are no precisely analogous structures to crypts. However, villus-like folds extend throughout the intestinal epithelium by 14 dpf and after about a month, proliferative cells are entirely restricted to the inter-villus regions and the intestine adopts a coiled configuration (for further characterization of the mature zebrafish intestine, see Crosnier et al., 2005; Wallace et al., 2005a).

Regional differences in the morphology and differentiation of the developing intestine suggest a nomenclature for its organization

In this paper, we propose to refine the nomenclature proposed by Field et al. (2003a) whereby the developing zebrafish intestinal tract is divided into two anatomically distinct regions: the intestinal bulb and posterior intestine. Here, we have built on previous observations in juvenile and adult stomachless teleost fish where, on the basis of regional differences in epithelial cell morphology and differentiation, three intestinal segments were distinguished (Noaillac-Depeyre and Gas, 1974, 1976; Stroband and Debets, 1978, Rombout et al., 1985). In the intestine of a freshwater teleost, the tench, ultrastructural studies revealed that enterocytes associated with the enlarged proximal segment contained absorbed fats in lipid particles and lipid droplets, identifying these cells as being concerned with lipid absorption (Noaillac-Depeyre and Gas, 1974, 1976). Notably, this region correlates with the tissue-specific expression pattern of the *ifabp* gene in zebrafish (Andre et al., 2000; Her et al., 2004). Cells in a shorter middle segment showed many invaginations and pinocytosis figures and large vacuoles in the supranuclear cytoplasm (Noaillac-Depeyre and Gas, 1976), features that have been shown to be characteristic of absorptive enterocytes (Gargiulo et al., 1998). Enterocytes in the distal segment showed a large mitochondrial population and numerous invaginations of the plasma membrane, consistent with a function in water and ion transport (Noaillac-Depeyre and Gas, 1976). Thus, the three segments in the mature cyprinid intestine appear to be the functional counterparts of the intestinal bulb, mid-intestine and posterior intestine that are first distinguished in the zebrafish intestine during the fourth day of development.

Characteristics of the different regions in the developing zebrafish intestine

The most conspicuous feature of the zebrafish intestine at 102 hpf is the intestinal bulb. In this rostral region of the intestine, the lumen has greatly expanded and the epithelial layer is thrown into folds. Meanwhile, the abundance of goblet cells and the presence of large supranuclear vacuoles in the enterocytes (see also Wallace et al., 2005a) distinguish the mid-intestine from the other two regions at 102 hpf. Indeed, until 12–14 dpf the mid-intestine is the sole site of goblet cell differentiation. Goblet cells are highly specialized epithelial cells that secrete mucus to cover the mucosal surface to protect cells against phagocytosis and dehydration. The mucus layer also provides a hydrophilic environment that plays a role in hormone and mitogen binding to cells and transportation of ions across the plasma membrane. It has been suggested that the specific secretion of acidic mucins in early life, as demonstrated here, may be of particular importance as an innate defense barrier. The acquired immune system is not fully functional yet (Deplancke and Gaskins, 2001) and acidic mucins appear to be more resistant to degradation by bacterial glycosidases. Several other observations reinforce the notion that the mid-intestine is functionally distinct from the other two regions. For example, the mid-intestine in zebrafish also appears to be involved in iron absorption. Expression of the iron transporter, ferroportin 1, mutated in the *weissherbst* (*weh*) mutant (Donovan et al., 2000) is confined to the mid-intestine in 6 dpf zebrafish larvae (Donovan and Zon, personal communication). However, a second iron transporter, Divalent metal transporter 1 (Dmt1), mutated in the *chardonnay* mutant (*cdy*), is expressed predominantly in the intestinal bulb (Donovan et al., 2002), indicating that iron absorption takes place in other regions of the intestine as well.

Introduction of the Tg[nkx2.2a:mEGFP] line for studies of intestinal endocrine cell development

The pattern of EGFP fluorescence in the ventral neural tube and developing pancreas of *Tg[nkx2.2a:mEGFP]* transgenic embryos is as expected and further highlights the usefulness of BAC clone recombination technology to produce transgenic organisms with predictable and authentic patterns of reporter gene expression (Shin et al., 2003; Schonhoff et al., 2004b). However, the appearance of EGFP-positive cells in the intestinal epithelium from 52 hpf was not predicted because *nkx2.2a* expression had not previously been investigated in this organ. Using in situ hybridization, we were able to demonstrate that *nkx2.2a* mRNA was localized in cells that had exactly the same frequency and distribution as the EGFP-positive cells in the intestinal epithelium of the *Tg[nkx2.2a:mEGFP]* line. Moreover, we demonstrated that a subpopulation of these cells expressed glucagon and somatostatin, thereby identi-

fying them as enteroendocrine cells. Enteroendocrine cells expressing pancreatic polypeptide have been previously identified in both the adult and embryonic zebrafish intestine (Langer et al., 1979; Wallace et al., 2005a,b) and recently a new monoclonal antibody, 2F11, that recognizes both goblet cells and enteroendocrine cells from 96 hpf, has also been described (Crosnier et al., 2005). In the mammalian intestine, there are thought to be at least fourteen different populations of enteroendocrine cells, each expressing a different hormone or combination of hormones (Schonhoff et al., 2004a). As more antibodies that cross-react with zebrafish gut hormones are identified, the range of hormones expressed by zebrafish enteroendocrine cells may be found to be similar to that of mammals.

Nkx2.2 is a homeodomain transcription factor whose non-redundant functions in oligodendrocyte differentiation and pancreatic β cell differentiation have been elegantly demonstrated by analysis of Nkx2.2-deficient mice (Qi et al., 2001; Sussel et al., 1998). However, to our knowledge, enteroendocrine cell development has not been studied in Nkx2.2-deficient mice, yet our results in zebrafish would predict that these cells are also likely to be affected. Indeed, the role, if any, of Nkx2.2 in vertebrate enteroendocrine cell specification and/or differentiation has yet to be elucidated. However, in amphioxus, the Nkx2.2 homologue, AmphiNK2.2, has been implicated in the regionalization of the early gut endoderm and in the differentiation of a sparse population of intensely positive *AmphiNK2.2*-expressing cells in the midgut epithelium (Holland et al., 1998). In adult amphioxus, scattered cells in the midgut epithelium have been shown to produce glucagon and insulin (Reinecke, 1981) but it is not known yet whether these are related to the cells that express Nkx2.2. In a recent study aimed at unraveling the molecular pathways involved in cell lineage determination in the mammalian pancreas, DNA microarray analysis was combined with a modified single-cell PCR procedure to study gene expression profiles of single pancreatic cells at E10.5 of development when the pancreatic epithelium is morphologically uniform (Chiang and Melton, 2003). This analysis allowed the authors to determine a transcription factor "code" characteristic of six different cell types (Types I to VI) that essentially described cells at all stages of cell lineage determination. Thus, cells with stem cell-like attributes were identified (Type I) along with a series of intermediate progenitors (Types II, III and IV) and highly differentiated cells that secreted hormones (Types V and VI). Interestingly, Nkx2.2 was unique in being expressed in all six-cell types, suggesting that Nkx2.2 may be a reliable (pan) marker of both developing and mature endocrine cells. This concept is consistent with our analysis of *nkx2.2a*/EGFP-positive cells in the developing intestine of *Tg[nkx2.2a:mEGFP]* embryos, where a subset of the *nkx2.2a*/EGFP-expressing cells express the hormones glucagon and somatostatin.

The GFP expression pattern in gutGFP fish is probably related to the transgenic construct integrating close to the foxA3/fkd2 gene

When the gutGFP transgenic line was first introduced by Field et al. (2003a), the authors commented that the expression pattern of GFP in the gutGFP line almost completely recapitulated that of *foxA3/fkd2* in developing zebrafish embryos. As well as expression throughout the endoderm, *foxA3/fkd2* is also noted for its expression in the hatching gland and notochord during the pharyngula period (Odenthal and Nusslein-Volhard, 1998). When we studied the GFP expression pattern at high resolution using anti-GFP antibodies, we found that every cell in the intestinal epithelium was GFP positive (data not shown). This finding is consistent with *foxA3/fkd2* expression in the intestinal epithelium of mice, where three intestinal cell lineages (enterocytes, goblet cells and enteroendocrine cells) express this endodermal marker (Liu et al., 2002).

To explore the mechanism responsible for the gutGFP expression pattern, we identified the site of integration of the EF1α-GFP construct in the zebrafish genome. The GFP coding sequence was precisely pinpointed to a position only 58 kb downstream from the 3′UTR of the *foxA3/fkd2* gene, albeit in the opposite orientation, with no intervening genes or open reading frames between the site of integration and the *foxA3/fkd2* gene. One interpretation of this result is that the construct integrated close to an orientation-independent enhancer element that normally regulates the tissue-specific expression of the *foxA3/fkd2* gene. Alternatively, it is possible that the open chromatin conformation that ensued upon transcription of the *foxA3/fkd2* gene was sufficient to hijack transcription of the GFP construct as well. Though the precise mechanism remains to be determined, it seems probable that the close proximity of the construct integration site to the *foxA3/fkd2* gene is related to the tissue-specific GFP expression pattern observed in the gutGFP line.

Characterization of mutants with defects in the zebrafish intestine

In this paper we present a systematic analysis of the morphogenetic events that take place during the formation of the zebrafish intestinal epithelium over the first 5 days of development, which we hope will be a useful reference for the characterization of current and future intestinal mutants. So far, little is known about the genetic mechanisms that govern the conversion of a flat layer of endoderm into an elaborately folded tubular epithelial monolayer containing polarized and differentiated cells. The cloning of zebrafish intestinal mutants such as *flo*, in which the intestinal epithelium exhibits defects in polarization, differentiation and cell survival, is likely to provide insights into this process. Two intestinal mutants have been cloned so far. The first, *nil per os* (*npo*), exhibits striking intestinal differ-

entiation abnormalities as a result of a mutation in a gene encoding a protein with an RNA recognition motif (Mayer and Fishman, 2003). The authors speculate that this RNA binding protein may regulate the stability of multiple mRNAs encoding proteins that govern intestinal differentiation (Mayer and Fishman, 2003). The second, *meltdown* (*mlt*), develops cystic expansion of the posterior intestine as a result of a gain-of-function mutation in the smooth muscle myosin heavy chain and demonstrates an essential role for smooth muscle in the maintenance of intestinal epithelial cell architecture (Wallace et al., 2005b). Focused screens including a histology-based screen (Mohideen et al., 2003) and the Liver^{plus} screen based on the gutGFP line discussed here (E. Ober, H.M Verkade, H.A Field, DD, DYRS et al., manuscript in preparation) have recently expanded the number of intestinal mutants available for study. We can therefore look forward to major advances in this field in the future.

Acknowledgments

The authors thank Val Feakes for histological expertise, Helen Abud for guidance with anti-active caspase 3 immunohistochemistry, Stephen Cody and Eva Tomaskovic-Crook for assistance with microscopy, Nathan Hall for bioinformatics support, Marjolein Blits for technical assistance and Janna Taylor for photography. Holly Field, Heather Verkade, Helen Abud and Tony Burgess provided insightful comments on the manuscript. The work was supported in part by a Dora Lush NHMRC postgraduate award to TADJ-C and project grant # 280916 from the NHMRC, Australia, to JKH. The Christopher Reeve Paralysis Foundation and the National Multiple Sclerosis Society supported the work conducted in the laboratory of BA. Confocal microscopy at Vanderbilt was performed using equipment made available by the Vanderbilt University Cell Imaging Core Resource, supported by NIH grants 1S10RR15682-1, CA68485 and DK20593.

References

Abud, H.E., Watson, N., Heath, J.K., 2005. Growth of intestinal epithelium in organ culture is dependent on EGF signalling. Exp. Cell Res. 303, 252–262.

Alexander, J., Stainier, D.Y., 1999. A molecular pathway leading to endoderm formation in zebrafish. Curr. Biol. 9, 1147–1157.

Amatruda, J.F., Shepard, J.L., Stern, H.M., Zon, L.I., 2002. Zebrafish as a cancer model system. Cancer Cell 1, 229–231.

Andre, M., Ando, S., Ballagny, C., Durliat, M., Poupard, G., Briancon, C., Babin, P.J., 2000. Intestinal fatty acid binding protein gene expression reveals the cephalocaudal patterning during zebrafish gut morphogenesis. Int. J. Dev. Biol. 44, 249–252.

Aoki, T.O., David, N.B., Minchiotti, G., Saint-Etienne, L., Dickmeis, T., Persico, G.M., Strahle, U., Mourrain, P., Rosa, F.M., 2002. Molecular integration of casanova in the Nodal signalling pathway controlling endoderm formation. Development 129, 275–286.

Barolo, S., Posakony, J.W., 2002. Three habits of highly effective signaling pathways: principles of transcriptional control by developmental cell signaling. Genes Dev. 16, 1167–1181.

Barth, K.A., Wilson, S.W., 1995. Expression of zebrafish nk2.2 is influenced by sonic hedgehog/vertebrate hedgehog-1 and demarcates a zone of neuronal differentiation in the embryonic forebrain. Development 121, 1755–1768.

Chang, H.Y., Yang, X., 2000. Proteases for cell suicide: functions and regulation of caspases. Microbiol. Mol. Biol. Rev. 64, 821–846 (Review).

Chen, J.N., Haffter, P., Odenthal, J., Vogelsang, E., Brand, M., van Eeden, F.J., Furutani-Seiki, M., Granato, M., Hammerschmidt, M., Heisenberg, C.P., Jiang, Y.J., Kane, D.A., Kelsh, R.N., Mullins, M.C., Nusslein-Volhard, C., 1996. Mutations affecting the cardiovascular system and other internal organs in zebrafish. Development 123, 293–302.

Chiang, M.K., Melton, D.A., 2003. Single-cell transcript analysis of pancreas development. Dev. Cell 4, 383–393.

Crosnier, C., Vargesson, N., Gschmeissner, S., Ariza-McNaughton, L., Morrison, A., Lewis, J., 2005. Delta-Notch signalling controls commitment to a secretory fate in the zebrafish intestine. Development 132, 1093–1104.

Dahl, U., Sjodin, A., Semb, H., 1996. Cadherins regulate aggregation of pancreatic beta cells in vivo. Development 122, 2895–2902.

Deplancke, B., Gaskins, H.R., 2001. Microbial modulation of innate defense: goblet cells and the intestinal mucus layer. Am. J. Clin. Nutr. 73, 1131S–1141S (Suppl.)

Dickmeis, T., Mourrain, P., Saint-Etienne, L., Fischer, N., Aanstad, P., Clark, M., Strahle, U., Rosa, F., 2001. A crucial component of the endoderm formation pathway, CASANOVA, is encoded by a novel sox-related gene. Genes Dev. 15, 1487–1492.

Donovan, A., Brownlie, A., Zhou, Y., Shepard, J., Pratt, S.J., Moynihan, J., Paw, B.H., Drejer, A., Barut, B., Zapata, A., Law, T.C., Brugnara, C., Lux, S.E., Pinkus, G.S., Pinkus, J.L., Kingsley, P.D., Palis, J., Fleming, M.D., Andrews, N.C., Zon, L.I., 2000. Positional cloning of zebrafish ferroportin1 identifies a conserved vertebrate iron exporter. Nature 403, 776–781.

Donovan, A., Brownlie, A., Dorschner, M.O., Zhou, Y., Pratt, S.J., Paw, B.H., Phillips, R.B., Thisse, C., Thisse, B., Zon, L.I., 2002. The zebrafish mutant gene chardonnay (cdy) encodes divalent metal transporter 1 (DMT1). Blood 100, 4655–4659.

Drummond, I.A., Majumdar, A., Hentschel, H., Elger, M., Solnica-Krezel, L., Schier, A.F., Neuhauss, S.C., Stemple, D.L., Zwartkruis, F., Rangini, Z., Driever, W., Fishman, M.C., 1998. Early development of the zebrafish pronephros and analysis of mutations affecting pronephric function. Development 125, 4655–4667.

Field, H.A., Ober, E.A., Roeser, T., Stainier, D.Y.R., 2003a. Formation of the digestive system in zebrafish, I. Liver morphogenesis. Dev. Biol. 253, 279–290.

Field, H.A., Si Dong, P.D., Beis, D., Stainier, D.Y.R., 2003b. Formation of the digestive system in zebrafish: II. Pancreas morphogenesis. Dev. Biol. 261, 197–208.

Ganz, T., 2003. Microbiology: gut defense. Nature 422, 478–479.

Gargiulo, A.M., Ceccarelli, P., Dall'Anglio, C., Pedini, V., 1998. Histology and ultrastructure of the gut of the tilapia (tilapia spp.), a hybrid teleost. Anat. Histol. Embryol. 27, 89–94.

Gordon, J.I., Hermiston, M.L., 1994. Differentiation and self-renewal in the mouse gastrointestinal epithelium. Curr. Opin. Cell Biol. 6, 795–803.

Grapin-Botton, A., Melton, D.A., 2000. Endoderm development from patterning to organogenesis. TIG 16, 124–130.

Haddon, C., Lewis, J., 1996. Early ear development in the embryo of the zebrafish *Danio rerio*. J. Comp. Neurol. 365, 113–128.

Hauptmann, G., Gerster, T., 2000. Multicolor whole-mount in situ hybridization. Methods Mol. Biol. 137, 139–148.

Her, G.M., Yeh, Y.H., Wu, J.L., 2004. Functional conserved elements mediate intestinal-type fatty acid binding protein (I-FABP) expression in the gut epithelia of zebrafish larvae. Dev. Dyn. 230, 734–742.

Holland, L.Z., Venkatesh, T.V., Gorlin, A., Bodmer, R., Holland, N.D., 1998. Characterization and developmental expression of AmphiNk2-2, an NK2 class homeobox gene from Amphioxus. Dev. Genes Evol. 208, 100–105.

Horne-Badovinac, S., Lin, D., Waldron, S., Schwarz, M., Mbamalu, G., Pawson, T., Jan, Y., Stainier, D.Y., Abdelilah-Seyfried, S., 2001. Positional cloning of *heart and soul* reveals multiple roles for PKC lambda in zebrafish organogenesis. Curr. Biol. 11, 1492–1502.

Kamisaka, Y., Fujii, Y., Yamamoto, S., Kurokawa, T., Ronnestad, I., Totland, G.K., Tagawa, M., Tanaka, M., 2003. Distribution of cholecystokinin-immunoreactive cells in the digestive tract of the larval teleost, ayu, *Plecoglossus altivelis*. Gen. Comp. Endocrinol. 134, 116–121.

Kikuchi, Y., Agathon, A., Alexander, J., Thisse, C., Waldron, S., Yelon, D., Thisse, B., Stainier, D.Y., 2001. casanova encodes a novel Sox-related protein necessary and sufficient for early endoderm formation in zebrafish. Genes Dev. 15, 1493–1505.

Kimmel, C.B., Ballard, W.W., Kimmel, S.R., Ullmann, B., Schilling, T.F., 1995. Stages of embryonic development of the zebrafish. Dev. Dyn. 203, 253–310.

Langer, M., Van Noorden, S., Polak, J.M., Pearse, A.G., 1979. Peptide hormone-like immunoreactivity in the gastrointestinal tract and endocrine pancreas of eleven teleost species. Cell Tissue Res. 199, 493–508.

Lee, E.C., Yu, D., Martinez de Velasco, J., Tessarollo, L., Swing, D.A., Court, D.L., Jenkins, N.A., Copeland, N.G., 2001. A highly efficient *Escherichia coli*-based chromosome engineering system adapted for recombination targeting and subcloning of BAC DNA. Genomics 73, 56–65.

Leung, B., Hermann, G.J., Priess, J.R., 1999. Organogenesis of the *Caenorhabditis elegans* intestine. Dev. Biol. 216, 114–134.

Liu, Y., Shen, W., Brubaker, P.L., Kaestner, K.H., Drucker, D.F., 2002. Foxa3 (HNF-3γ) binds to and activates the rat proglucagon gene promoter but is not essential for proglucagon gene expression. Biochem. J. 366, 633–641.

Lubarsky, B., Krasnow, M.A., 2003. Tube morphogenesis: making and shaping biological tubes. Cell 112, 19–28.

Lunde, K., Belting, H.G., Driever, W., 2004. Zebrafish *pou5f1/pou2*, homolog of mammalian *Oct4*, functions in the endoderm specification cascade. Curr. Biol. 14, 48–55.

Mathan, M., Moxey, P.C., Trier, J.S., 1976. Morphogenesis of fetal rat duodenal villi. Am. J. Anat. 146, 73–92.

Mayer, A.N., Fishman, M.C., 2003. *nil per os* encodes a conserved RNA recognition motif protein required for morphogenesis and cytodifferentiation of digestive organs in zebrafish. Development 130, 3917–3928.

Mohideen, M.P.K., Beckwith, L.G., Tsao-Wu, G.S., Moore, J.L., Wong, A.C.C., Chinoy, M.R., Cheng, K.C., 2003. Histology-based screen for zebrafish mutants with abnormal cell differentiation. Dev. Dyn. 228, 414–423.

Montuenga, L.M., Guembe, L., Burrell, M.A., Bodegas, M.E., Calvo, A., Sola, J.J., Sesma, P., Villaro, A.C., 2003. The diffuse endocrine system: from embryogenesis to carcinogenesis. Progr. Histochem. Cytochem. 38, 155–272.

Neves, C.A., Gitirana, L.B., Serrao, J.E., 2003. Ultrastructure of the midgut endocrine cells in *Melipona quadrifasciata anthidiodes* (Hymenoptera Apidae). Braz. J. Biol. 63, 683–690.

Noaillac-Depeyre, J., Gas, N., 1974. Fat absorption by the enterocytes of the carp (*Cyprinus carpio* L.). Cell Tissue Res. 155, 353–365.

Noaillac-Depeyre, J., Gas, N., 1976. Electron microscopic study on gut epithelium of the tench (*Tinca tinca* L.) with respect to its absorptive functions. Tissue Cell 8, 511–530.

Ober, E.A., Field, H.A., Stainier, D.Y., 2003. From endoderm formation to liver and pancreas development in zebrafish. Mech. Dev. 120, 5–18.

Odenthal, J., Nusslein-Volhard, C., 1998. Forkhead domain genes in zebrafish. Dev. Genes Evol. 208, 245–258.

Oving, I.M., Clevers, H.C., 2002. Molecular causes of colon cancer. Eur. J. Clin. Invest. 32, 448–457.

Pack, M., Solnica-Krezel, L., Malicki, J., Neuhauss, S.C., Schier, A.F., Stemple, D.L., Driever, W., Fishman, M.C., 1996. Mutations affecting development of zebrafish digestive organs. Development 123, 321–328.

Pan, Q.S., Fang, Z.P., Zhao, Y.X., 2000. Immunocytochemical identification and localization of APUD cells in the gut of seven stomachless teleost fishes. World J. Gastroenterol. 6, 96–101.

Qi, Y., Cai, J., Wu, Y., Wu, R., Lee, J., Fu, H., Rao, M., Sussel, L., Rubenstein, J., Qiu, M., 2001. Control of oligodendrocyte differentiation by the Nkx2.2 homeodomain transcription factor. Development 128, 2723–2733.

Reim, G., Mizoguchi, T., Stainier, D.Y., Kikuchi, Y., Brand, M., 2004. The POU domain protein (pou2/Oct4) is essential for endoderm formation in cooperation with the HMG domain protein casanova. Dev. Cell 6, 91–101.

Reinecke, M., 1981. Immunohistochemical localization of polypeptide hormones in endocrine cells of the digestive tract of *Branchiostoma lanceolatum*. Cell Tissue Res. 219, 445–456.

Rombout, J.H.W.M., Stroband, H.W.J., Taverne-Thiele, J.J., 1984. Proliferation and differentiation of intestinal epithelial cells during development of *Barbus conchionius* (Teleostei Cyprinidae). Cell Tissue Res. 236, 207–216.

Rombout, J.H.W.M., Lamers, C.H.J., Helfrich, M.H., Taverne-Thiele, J.L., 1985. Uptake and transport of intact macromolecules in the intestinal epithelium of carp (*Cyprinus carpio* L.) and the possible immunological implications. Cell Tissue Res. 239, 519–530.

Rugendorff, A., Younossi-Hartenstein, A., Hartenstein, V., 1994. Embryonic origin and differentiation of the *Drosophila* heart. Roux's Arch. Dev. Biol. 203, 266–280.

Sancho, E., Batlle, E., Clevers, H., 2003. Live and let die in the intestinal epithelium. Curr. Opin. Cell Biol. 15, 1–8.

Schäfer, M., Kinzel, D., Neuner, C., Schartl, M., Volff, J.-N., Winkler, C., 2005. Hedgehog and retinoid signalling confines *nkx2.2b* expression to the lateral floor plate of the zebrafish trunk. Mech. Dev. 122, 43–56.

Schier, A.F., 2003. Nodal signaling in vertebrate development. Annu. Rev. Cell Dev. Biol. 19, 589–621.

Shepherd, I.T., Pietsch, J., Elworthy, S., Kelsh, R.N., Raible, D.W., 2004. Roles for GFRα1 receptors in zebrafish enteric nervous system development. Development 131, 241–249.

Shin, J., Park, H.-C., Topczewska, J.M., Mawdsley, D.J., Appel, B., 2003. Neural cell fate analysis in zebrafish using *oligo2* BAC transgenics. Methods Cell Sci. 25, 7–14.

Schonhoff, S.E., Giel-Moloney, M., Leiter, A.B., 2004a. Development and differentiation of gut endocrine cells. Endocrinology 145, 2639–2644.

Schonhoff, S.E., Giel-Moloney, M., Leiter, A.B., 2004b. Neurogenin 3-expressing progenitor cells in the gastrointestinal tract differentiate into both endocrine and non-endocrine cell types. Dev. Biol. 270, 443–454.

Stainier, D.Y.R., 2002. A glimpse into the molecular entrails of endoderm formation. Genes Dev. 16, 893–907.

Stainier, D.Y., Fouquet, B., Chen, J.N., Warren, K.S., Weinstein, B.M., Meiler, S.E., Mohideen, M.A., Neuhauss, S.C., Solnica-Krezel, L., Schier, A.F., Zwartkruis, F., Stemple, D.L., Malicki, J., Driever, W., Fishman, M.C., 1996. Mutations affecting the formation and function of the cardiovascular system in the zebrafish embryo. Development 123, 285–292.

Strahle, U., Blader, P., 1994. Early neurogenesis in the zebrafish embryo. FASEB J. 8, 692–698.

Stroband, H.W.J., Debets, F.M.H., 1978. The ultrastrucutre and renewal of the intestinal epithelium of the juvenile Grasscarp (*Ctenopharyngodon idella* (Val.)). Cell Tissue Res. 187, 181–200.

Sussel, L., Kalamaras, J., Hartigan-O'Connor, D.J., Meneses, J.J., Pedersen, R.A., Rubenstein, J.L., German, M.S., 1998. Mice lacking the homeodomain transcription factor Nkx2.2 have diabetes due to arrested differentiation of pancreatic beta cells. Development 125, 2213–2221.

Tam, P.P., Kanai-Azuma, M., Kanai, Y., 2003. Early endoderm development in vertebrates: lineage differentiation and morphogenetic function. Curr. Opin. Genet. Dev. 4, 393–400.

Wallace, K.N., Pack, M., 2003. Unique and conserved aspects of gut development in zebrafish. Dev. Biol. 255, 12–29.

Wallace, K.N., Akhter, S., Smith, E.M., Lorent, K., Pack, M., 2005a. Intestinal growth and differentiation in zebrafish. Mech. Dev. 122, 157–173.

Wallace, K.N., Dolan, A.C., Seiler, C., Smith, E.M., Yusuff, S., Chaille-Arnold, L., Judson, B., Slerk, R., Yengo, C., Sweeney, H.L., Pack, M., 2005b. Mutation of smooth muscle myosin causes epithelial invasion and cystic expansion of the zebrafish intestine. Dev. Cell 8, 717–726.

Warga, R.M., Kimmel, C.B., 1990. Cell movements during epiboly and gastrulation in zebrafish. Development 108, 569–580.

Warga, R.M., Nusslein-Volhard, C., 1999. Origin and development of the zebrafish endoderm. Development 126, 827–838.

Warga, R.M., Stainier, D.Y., 2002. The guts of endoderm formation. Results Probl. Cell Differ. 40, 28–47.

Wells, J.M., Melton, D.A., 1999. Vertebrate endoderm development. Annu. Rev. Cell Dev. Biol. 15, 393–410.

Whitfield, T.T., Riley, B.B., Chiang, M.-Y., Phillips, B., 2002. Development of the zebrafish inner ear. Dev. Dyn. 223, 427–458.

Yang, Q., Bermingham, N.A., Finegold, M.J., Zoghbi, H.Y., 2001. Requirement of Math1 for secretory cell lineage commitment in the mouse intestine. Science 294, 2155–2158.